Review

DISCRETE MODELS FOR CHEMICALLY REACTING SYSTEMS

Raymond KAPRAL

Chemical Physics Theory Group, Department of Chemistry, University of Toronto, Toronto, Ontario M5S 1A1, Canada

Abstract

Nonequilibrium spatially distributed chemically reacting systems are usually described in terms of reaction–diffusion equations. In this article, a hierarchy of discrete models is studied that show similar spatio-temporal structure and can be used to explore the complex phenomena occurring in these systems. We consider cellular automaton models where space, time and chemical concentrations are discrete and the dynamics is embodied in a simple updating rule, coupled map lattices where space and time are discrete variables but chemical concentrations are continuous and the dynamics is given by a nonlinear function and, lastly, lattice gas cellular automaton models that view the system on a microscopic or mesoscopic level where space, time and particle velocities are discrete.

1. Introduction

In the macroscopic regime, the spatio-temporal dynamics of chemically reacting systems is described by reaction–diffusion equations of the general form

$$\frac{\partial c(r, t)}{\partial t} = R\left(c(r, t)\right) + D \cdot \nabla^2 c(r, t), \qquad (1.1)$$

where $c(r, t)$ is a vector of local concentration variables, R is a vector-valued function that describes local chemical reactions, and the last term accounts for diffusion of the chemical species. In the far-from-equilibrium domain which will concern us here, the reaction–diffusion equation can describe a rich variety of bifurcation structures that occur in macroscopic reacting systems. These include multi-stable states, oscillations, chemical waves and chemical chaos [1].

Most examples of the reaction–diffusion systems studied in this paper actually fall into three variants of (1.1). There are propagator–controller systems [2] that consitute a generic model of excitable media, the time-dependent Ginzburg–Landau model for a system with a non-conserved order parameter (model A) [3] that describes a class of chemical reactions which possess bistable steady states and, finally, the complex Ginzburg–Landau model [4,5] which can be used to study the onset of oscillations that arise from the Hopf bifurcation of a steady state. Much of the discussion in the subsequent sections will center on the phenomena embodied in these general equations, but other models will also be considered.

The subject of this review is the description of spatio-temporal structures in terms of even simpler discrete models of spatially-distributed chemically reacting systems. We consider a hierarchy of discrete models. At the simplest level are cellular automaton models where space, time and chemical concentrations are discrete and the reactive and diffusive dynamics are represented schematically by a rule for updating these discrete variables. Next in complexity are coupled map lattices where the space and time variables are discrete but concentrations may take on a continuum of values. Both of these models are abstractions of the reaction–diffusion equation (1.1). Lastly, we study a class of stochastic discrete models that treat the system at the molecular level (or perhaps, more accurately, at the mesoscopic level). These are lattice gas cellular automata where space, time and particle velocities are taken to be discrete variables. This last class of models has the added feature that fluctuations are incorporated, albeit in an approximate fashion, so that a description that goes beyond the reaction–diffusion equation is possible.

Since all of these models approximate the dynamics in some way, not all details of chemical pattern formation processes can be faithfully reproduced. Hence, the goal of such descriptions is to model the robust features of the spatio-temporal dynamics by simple, computationally efficient schemes that provide insight into the essential aspects of such nonlinear reacting systems.

A word about notation is in order: in this review, the notation in each major section is internally consistent but there may be duplication of symbols when different sections are compared. Since certain notation is standard in different fields of research, this compromise avoids the introduction of unusual symbols.

2. Cellular automaton models

Cellular automaton (CA) models for complex dynamical systems were devised by Von Neumann and Ulam in an attempt to construct a self-reproducing system that mimics biological evolution [6]. Recently, there has been a revival of interest in such models.

A cellular automaton model for a dynamical system can be constructed according to the following prescription. The dynamics is assumed to take place on an array of cells. Each cell can take on a finite number n of values in the set $S = \{s_m; m = 1, \ldots, n\}$. Dynamical evolution occurs according to a rule $\mathcal{R}$ that specifies how each cell changes its value from one discrete time to the next; in general, the upating rule depends on the value of s_m in the given cell as well as that of neighboring cells. The rule $\mathcal{R}$ may be deterministic or probabilistic in character. This seemingly simple set of operations can give rise to very complicated dynamics; in fact, it can be shown that rules can be constructed that are capable of universal computation; they are Turing machines.

The self-reproducing CA of Von Neumann was very complicated, consisting of twenty-nine states with complex updating rules, but simpler self-reproducing CA models have been constructed. For example, Codd has devised a simple eight-state automaton that accomplishes self-reproduction [7]. Recent activity has focused, for example, on the classification of cellular automaton rules according to the types of dynamics they produce,

their connection with formal language theory and statistical mechanics, etc. [8], which has helped to organize the study of such systems. In addition, there has been a wealth of applications of these models to problems in biology, physics and chemistry. Much of this recent activity stems from developments in computers which make simulations of such systems feasible and from advances in the field of nonlinear dynamics [9].

The focus of this section is not on such general aspects of CA models; rather, we consider how specific features of a certain class of chemically reacting systems can be described in terms of simple cellular automata. We first consider chemical systems that are excitable; i.e. they possess a stable resting state which exhibits the following response to perturbations: a small displacement from the resting state will relax directly back to that state, but if the magnitude of the perturbation exceeds some threshold value, the system will make a large excursion in phase space before returning to the resting state. During this excursion, the system is insensitive to further perturbation, i.e. refractory. Following this discussion of excitable media, we briefly describe the application of CA models to other types of reacting systems.

For an excitable system, the local dynamics is conveniently discussed in terms of the kinetics of two chemical concentrations u and v which satisfy the coupled rate laws [2]

$$\tau \frac{\mathrm{d}u}{\mathrm{d}t} = f(u, v), \qquad \frac{\mathrm{d}v}{\mathrm{d}t} = g(u, v), \qquad (2.1)$$

where τ is assumed to be small and f and g are functions with the general shapes sketched in fig. 1. The function f has a sigmoidal shape, while g has no extrema and intersects f as shown in the figure, giving rise to a stable fixed point. Often-used functional forms
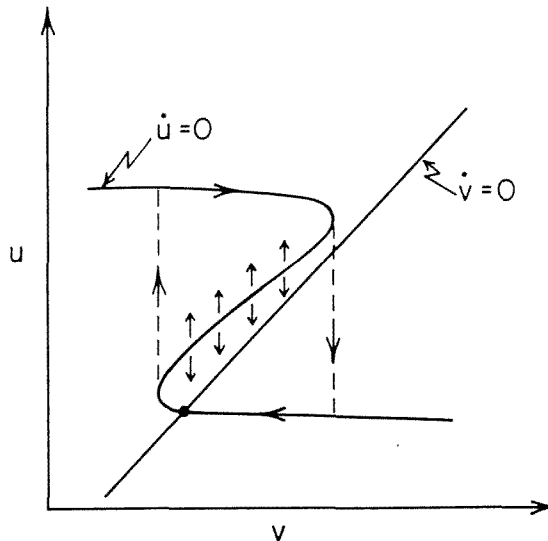

Fig. 1. Sketch of the $\dot{u} = 0$ and $\dot{v} = 0$ nullclines for an excitable system. The heavy dot indicates the stable fixed point and the arrows give the direction of the flow of the vector field.

with these general properties are $f(u, v) = -u^3 + \varepsilon u - v$ and $g(u, v) = u - av + b$. The flow of the vector field is as indicated in the figure. If the system is at the fixed point, it is stable to small perturbations; however, if the perturbation is sufficient to excite the phase point above the middle branch of the $\dot{u} = 0$ nullcline, then the system will execute a long excursion following the upper and lower branches of this nullcline except for the regions where it hops between branches. The time scale of the dynamics is governed by the parameter τ so that for small τ, u is a fast (propagator) variable while v is a slow (controller) variable. These are the main features of excitable kinetics which arise from the interplay of the two chemical species coupled by the reaction term with the characteristics described above. The spatially distributed version of a system with such local excitable kinetics constitutes an excitable medium and the propagator–controller equations for the medium are:

$$\tau \frac{\partial u(r, t)}{\partial t} = f\Big(u(r, t), v(r, t)\Big) + D_u \nabla^2 u(r, t),$$

$$\frac{\partial v(r, t)}{\partial t} = g\Big(u(r, t), v(r, t)\Big) + D_v \nabla^2 v(r, t). \tag{2.2}$$

There exist excellent reviews [2,10,11] and books [12] dealing with the properties of such systems. In the following subsections, we describe how the general features of this kind of dynamics can be captured by even simpler discrete models. The strategy is to replace the real concentration field (u, v) by a discrete variable or variables with local kinetics characteristic of excitability and coupling among these local discrete variables that accounts for the effects of diffusion.

2.1. SIMPLE EXCITABLE MEDIUM CA

First, a very simple CA model will be described that mimics the behavior of excitable media. Very roughly, the dynamical state of a system that satifies the rate law (2.1) can be classified as either resting (quiescent) Q, excited E, or refractory R. This crude classification can form the basis for a cellular automaton model of the dynamics. In fact, some of the earliest work on cellular automata has recognized and used this classification of states for the construction of the CA rules [6,13]. In the simplest CA models, the state of the system is represented by a single notional discrete concentration variable that can take on values corresponding to the above classification. Naturally, at this level of description any direct relation to the real concentration fields is lost.

In this simplest version of the excitable medium CA, the state space S is taken to be composed of the three states $S = \{Q, R, E\}$ and the cells occupy the nodes of a d-dimensional simple cubic lattice labeled by an index $i = (i_1, i_2, \ldots, i_d)$, $i_k \in \mathbb{Z}$. The excitable medium updating rule $\mathcal{R}_{em}$ is constructed to mimic the dynamics of the real system. Consider a cell isolated from interaction with its neighbors. If it is in the state Q, it will remain there since Q is the resting state. If the cell is excited, then in the two subsequent time steps it will become refractory and quiescent, $E \rightarrow R \rightarrow Q$, since an

excited system will return to the resting state. Let $j \in \mathcal{N}$, where $\mathcal{N}$ is a set of nodes defining the neighborhood of a given cell i. Diffusive interactions and excitability are taken into account by requiring the state of a cell i to depend on that of its neighbors j. If a cell is in Q and any of its nearest neighbors are in E, then the cell will become E in the next time step. If the cell is in R, then it is refractory and is unaffected by the state values of its neighbors. Thus, if we let $s(i, t)$ label the state of cell i at time t, we have the following deterministic updating rule:

$$\mathcal{R}_{em} : s(i, t+1) = \begin{cases} E & \text{if } s(i,t) = Q \text{ and } s(j,t) = E, \\ R & \text{if } s(i,t) = E, \\ Q & \text{if } s(i,t) = R \text{ or } s(i,t) = Q \text{ and } s(j,t) \in \{Q, R\}. \end{cases} \tag{2.1.1}$$

This very simple rule can reproduce many of the general features of chemical wave propagation in excitable systems. Three general types of chemical waves are observed in two-dimensional excitable media. *Rings* of excitation can be produced by a localized perturbation in a quiescent medium. The excitation will propagate outward at constant velocity as the perturbation excites the unperturbed surrounding medium. The refractory tail prevents back-propagation of the excitation, giving rise to a ring with increasing diameter whose thickness is determined by the length of the refractory period (one lattice site in this simplest model). If a periodic perturbation is applied locally (pacemaker), then *target patterns* may be formed by subsequent excitation of the quiescent medium within the rings of excitation. Provided the recovery time of the medium is short compared to the period of excitation, the frequency of the chemical waves in the target patterns will be that of the pacemaker. Perhaps the most interesting chemical waves that form in such media are *spiral waves*. Experimentally, these can be produced by tilting a dish of chemical reagent that supports rings or target patterns; shearing them produces lines of excitation whose free ends form the cores of spiral waves [14]. Alternatively, inhomogeneities intrinsic to the medium can provide a mechanism for the fragmentation of rings and subsequent formation and break-up of spiral waves. For example, see refs. [13, 15–18].

Consideration of the evolution of the excitable medium CA shows that an initial condition corresponding to an excited cell in a sea of quiescent cells will evolve to an expanding "ring" of excitation, but with the geometry of the underlying lattice (fig. 2(a)). This feature precludes the study of phenomena that depend on the curvature of the spatial pattern. We shall return to this point later in the discussion of more complex excitable medium CA models and coupled map lattices. If the ring is sheared, the free ends curl around to form a pair of counter-rotating spiral waves, just as in a real excitable medium. The spiral geometry arises from the fact that a line of excited cells is "protected" on one side by a line of refractory cells, forcing the excitation to wind around the free end. This is the discrete analog of the corresponding process that occurs in reaction–diffusion models [10, 11, 19–23]. The evolution of a spiral wave from a line-like initial condition is shown in fig. 2(b) and an example of the evolution that results from broken "rings"
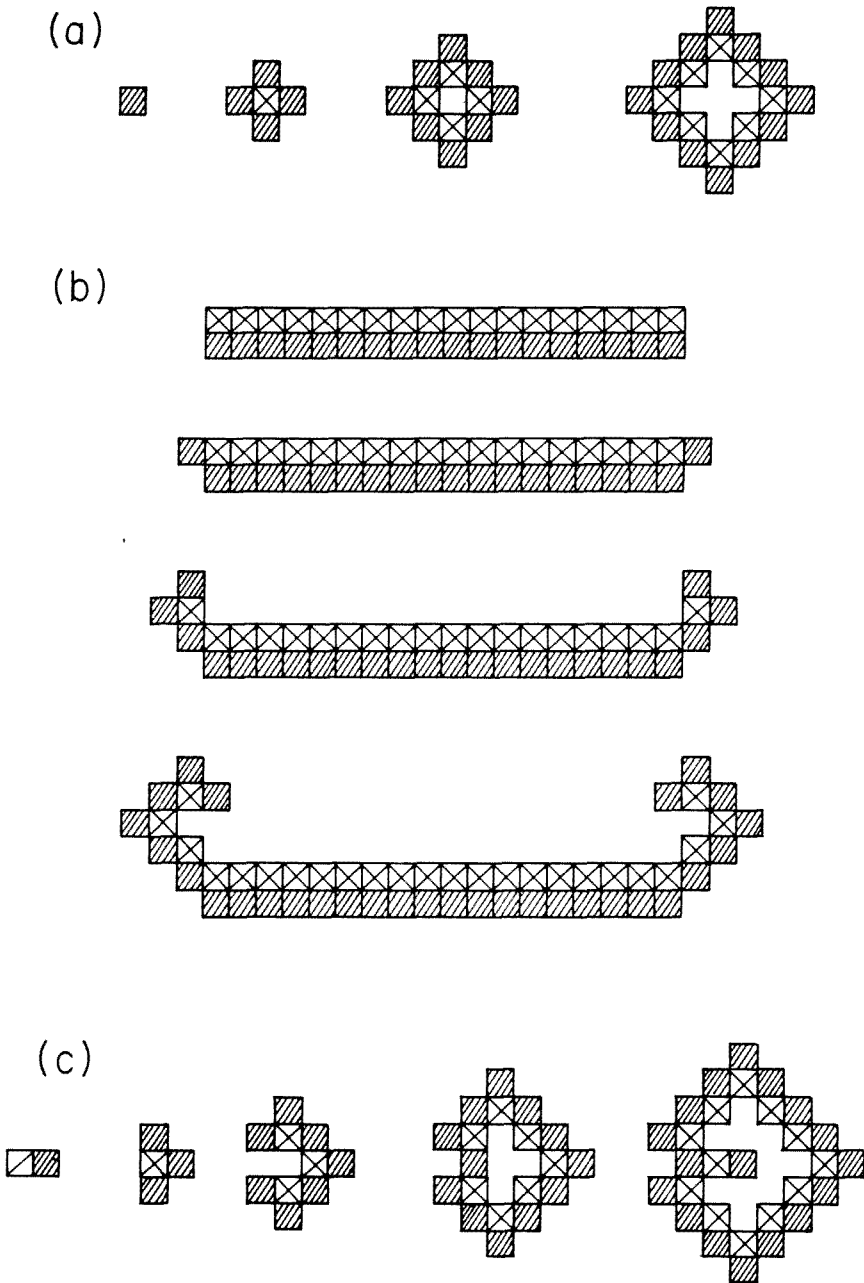
Fig. 2. Excitable medium CA wave propagation:
(a) ring; (b) spiral wave; (c) "target" pattern.

is shown in fig. 3. Note again that the spiral wave assumes a geometry consistent with the underlying lattice. The core of the spiral wave is pinned to a given location in the lattice and consists of the cycling configuration of cells shown in fig. 4; hence, the spiral
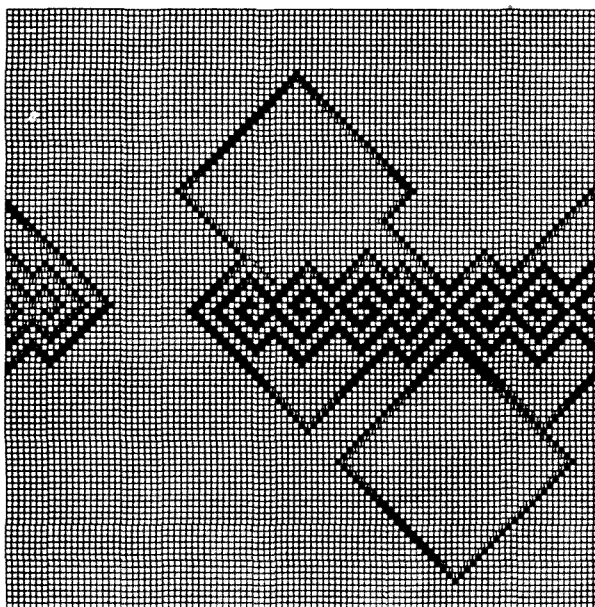
Fig. 3. Formation of spiral waves in the excitable medium CA following the shearing of "rings" of excitation.
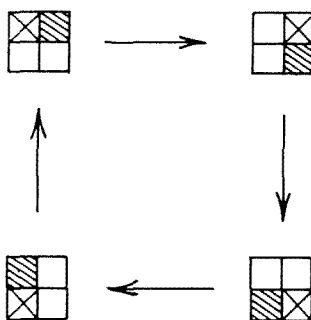

Fig. 4. Cycling configuration of cells at the "core" of the excitable medium CA spiral.

core is a highly simplified version of the complex concentration gradients that are known to occur there. As a result of this simplified description, those properties that depend on the details of the nature of the chemical gradients in the core [24] or the motion [14,25–29] of the core are outside the scope of such a model. Finally, starting from an initial configuration consisting of an excited cell adjacent to a refractory cell in a quiescent medium, structures reminiscent of target patterns can be generated (fig. 2(c)). However, since the initial configuration is just that of the spiral core, these chemical waves are really a pair of spiral waves that have coalesced and the re-excitation

mechanism to form the pattern is presumably different from that in systems where an autonomous pacemaker arises from a local inhomogeneity or some other mechanism.

In three dimensions, new types of chemical waves appear [11, 30] and the excitable medium CA [31] has been used to investigate various problems, such as the initial conditions that can give rise to these waves, in an effort to determine how such waves can be produced in the laboratory.

The existence of the cyclic configuration of cells shown in fig. 4 is the key to understanding the asymptotic dynamics of this three-state automaton starting from random initial conditions in two dimensions. These configurations form the "nuclei" of periodic structures that govern the eventual dynamics of the system which consists of a random distribution of competing centers of periodic structures. Some aspects of continuous random initial seeding and the dynamical evolution on fractals have been studied for the three-state automaton, and demonstrate the additional complexities that arise for such initial states [32]. We shall comment further on random initial conditions in section 2.2.

While the evolution from random initial conditions containing all types of sites is quite complicated, if the initial state is taken to be a random distribution of excited cells in a quiescent medium, the evolution can be described quite simply. This case is not without interest, since many nucleation and growth processes evolve from this type of initial state. Also, many problems related to pattern formation processes in such media have a statistical character and their investigation entails averages over many realizations of the evolution process. In such circumstances, provided one is interested in gross aspects of the dynamics, these simple CA models can provide insight into the understanding of these more complicated problems. Below, we give an illustration of such an analysis and also relate certain aspects of chemical wave propagation in excitable media to percolation problems, a connection which may be useful in some circumstances.

Consider the CA evolution from an initial state where each cell independent of its neighbors is excited (assigned the value E) with probability p or quiescent (assigned the value Q) with probability $1 - p$ [33]. The E cells will form random clusters in the sea of quiescent cells and one can consider properties related to these clusters like their average size and distribution, just as in percolation theory [34]. Since E cells will excite their quiescent neighbors in subsequent time steps, we actually have a dynamical version of the percolation problem to consider. Below, we review a number of aspects of this behavior and show how it provides insight into features that arise in the evolution of chemical waves.

Depending on the value of p and the definition of the neighborhood $\mathcal{N}$, either the E cells or the Q cells (or both) will belong to a percolating cluster. To be specific, consider the Moore neighborhood consisting of the eight neighbors of a site so that the CA is defined on a square-matching lattice. On this lattice, the critical percolation probability [34] for E cells is $p_c = 0.407$, so for $p < p_c$ the E cells do not percolate but the Q cells do; also, by symmetry, for $p > 1 - p_c = 0.593$ the Q cells do not percolate but the E cells do. Hence, for $0.407 < p < 0.593$, both E and Q cells belong to percolating clusters.

Cellular automaton evolution gives rise to a dynamical version of this problem [33]. As described above, an isolated E cell in a quiescent medium will spawn a ring (square) of $8t$ excited cells at time t ($t > 0$) whose interior is protected by a ring of $8(t-1)$ ($t > 1$) refractory R cells. Thus, if $p < p_c$ at $t = 0$ so that E cells do not percolate, they may form part of a percolating cluster at some later time. A percolating cluster of excited cells at $t = 2$ is shown in fig. 5. A complication arises since the rings of
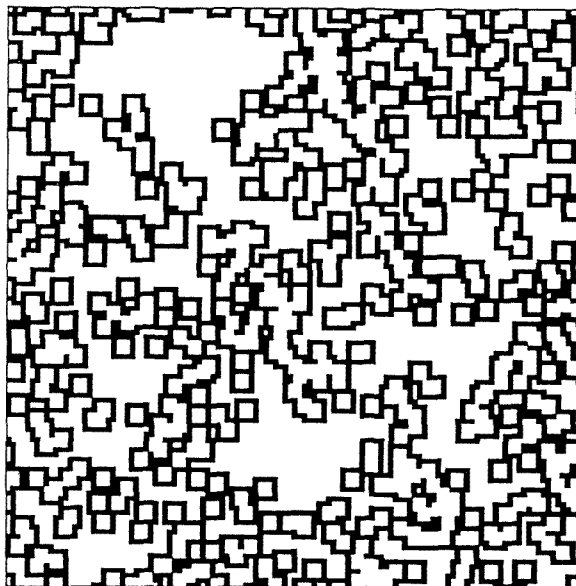

Fig. 5. A percolating cluster of excited cells at $t = 2$.
The critical percolation probability is $p_c(t = 2) = 0.41528$
(cf. ref. [33]).

excitation will collide and portions of the wavefronts will be annihilated. Alternatively, one may imagine that independently growing rings of excitation cover an area corresponding to a set of growing squares which in general overlap. We denote the area covered by these growing squares the *transformed area* and the E cells form the perimeter of this area. In the dynamical percolation problem, one quantity of interest is $p_c(t)$, the value of the initial seeding probability which gives rise to E cell percolation at time t. From the above description of the evolution, it is clear that the dynamical percolation problem is isomorphic to that of the percolation of a set of squares with sides $2t + 1$ (circles in the real system) [33,35]. Thus, a number of aspects of the dynamics of chemical wave formation in excitable media can be analyzed in terms of the language familiar from percolation theory. Additional scaling relations may be derived and questions related to the fractal dimensions of the growing patterns can be addressed easily for the automaton model [33].

The average transformed area (or volume) fraction $n(t)$ may also be easily computed for the CA with this type of initial seeding. In view of the independent random seeding process giving rise to the initial configuration and the deterministic nature of the growth process, the following argument may be used to determine $n(t)$ for a d-dimensional lattice [36]. An initially quiescent cell will become excited within the time t only if it lies within a volume $(2t + 1)^d$ surrounding an initially excited cell; the excited cell will produce a shell of excitation which covers this volume in a time t, so will certainly excite any cell lying within it. Since the probability that a randomly chosen cell is excited at $t = 0$ is p, the probability that a randomly chosen cell is untransformed (remains quiescent) at time t is $(1 - p)^{(2t + 1)^d}$. Hence, the average fraction transformed at time t is

$$n(t) = 1 - (1 - p)^{(2t + 1)^d}. \tag{2.1.2}$$

Since the excited cells constitute the surface of the transformed volume, the average fraction of the system which is excited at time t is just

$$n(t) - n(t - 1) = (1 - p)^{(2t - 1)^d} - (1 - p)^{(2t + 1)^d}. \tag{2.1.3}$$

This formula provides an exact result for the average number of excited cells in the system at time t or, in other terms, the average fraction of the excitable medium covered by wavefronts at time t.

Equation (2.1.3) is the discrete analog of the Johnson–Mehl–Avrami (JMA) [37] formula derived earlier in the study of nucleation and growth processes; clearly, the chemical wave propagation process may be considered from this point of view. For the type of random initial state described above, the JMA result is easily derived for disc (in 2-d) or spherical (in 3-d) wave propagation with constant velocity v in a continuous medium. The transformed volume fraction at time t is

$$n(t) = 1 - e^{-pV_d t^d}, \tag{2.1.4}$$

where $V_2 = \pi v^2$ and $V_3 = 4\pi v^3/3$, while the fraction of the system in the excited state $S_E(t)$ is just the perimeter (surface) of the average transformed area (volume)

$$S_E(t) = \dot{n}(t) = pdV_d t^{d-1} e^{-pV_d t^d}. \tag{2.1.5}$$

Since wavefronts in excitable media are often characterized by sharp concentration gradients, $S_E(t)$ can be measured in real systems by optical means.

It is also possible to generalize the CA model to allow for finite system size effects and effects due to inhomogeneous initial seeding. This allows a broader class of nucleation growth processes to be studied [38].

2.2. EXCITABLE MEDIUM CA: VARIATIONS ON THE THEME

The three-state excitable medium CA described above is perhaps the simplest model of a general class of excitable medium CA models. The apparently straightfoward generalization of this excitable medium CA to situations where E is a set of k excited states, $E = \{E_1, E_2, \ldots, E_k\}$ and R stands for a set of l refractory states, $R = \{R_1, \ldots, R_l\}$ produces amazingly rich behavior for evolution from random initial states [39]. The CA rule can be constructed as follows: suppose there are a total of n states, often referred to as "colors", in the automaton. We may label the states of the automaton by n integers, $\{Q, E_1, E_2, \ldots, E_k, R_1, R_2, \ldots, R_l\} = \{0, 1, 2, \ldots, n-1\}$. The number k can serve as a generalization of the simple threshold in the three-state automaton. If the state of a cell i at time t is $s(i, t) = m, m \geq k$, it will become $s(i, t) + 1$ (mod n) at the next time step regardless of the state of its neighbors. However, if $s(i, t) = m, m < k$, then the updating depends on its neighbors; it will change to $m + 1$ only if one of its neighbors is in $m + 1$. More formally, the CA rule is:

$$s(i, t+1) = \begin{cases} (s(i, t) + 1)\text{mod } n & \text{if } s(i, t) \geq k \text{ or } (s(i, t) + 1)\text{mod } n = s(j, t), \\ s(i, t) & \text{otherwise,} \end{cases} \quad (2.2.1)$$

where, as usual, $j \in \mathcal{N}$. The CA rule is thus a function of the number of states n, the threshold k, as well as the neighborhood $\mathcal{N}$. This model is often called the Greenberg–Hastings (GH) model [40]. It has been thoroughly studied by Fisch, Gravner and Griffeath [39]. They have examined the ergodic properties of the model in 1-d and have given a discussion of the conditions necessary for the formation of persistent patterns in 2-d. The model is able to produce a wide-range dynamical behavior, only some of which is analogous to that found in real excitable media. These studies can provide the theoretical underpinning of the dynamics of all the excitable medium CA models described here.

A related class of cyclic CA models has also been investigated and accounts of their properties have been given by Griffeath [41]. Such models may also have relevance for excitable chemical media.

In addition to these general but abstract versions of the excitable medium CA, there has been a number of studies that have considered more complex versions of the excitable medium CA model in order to study specific applications to chemically reacting media. As noted above, one of the main defects of the simple three-state model is the fact that chemical waves reflect the geometry of the underlying lattice. This precludes the investigation of phenomena which for their existence depend on the curvature of the wavefront. The nature of the pattern formation and growth in real excitable media often involves a delicate interplay between the nonlinear kinetics and the curvature effects that arise from the diffusion term in the reaction–diffusion equation [10, 11, 19–23]. We now describe how the excitable medium CA model has been generalized to incorporate wave curvature and wave dispersion.

Markus and Hess [42] have carried out detailed studies of wave propagation in an excitable medium CA model that incorporates both curvature and dispersion effects. The model has elements which are like those described above, but there is an essential difference in the way sites are placed on the lattice and the neighborhood is determined. The state space is the same as above for the GH model: there are n states $S = \{0, 1, \ldots, n - 1\}$, with 0 the resting state and a threshold for excitability k. Consider two space dimensions. The simple square lattice L is taken to be composed of N squares with sides of length q. Rather than occupying the nodes of the square lattice, the CA cells are now located at random positions within each square of L, one CA cell per square of L. We again label the CA cells by i. The neighborhood $\mathcal{N}$ of a cell i is defined as follows: a circle with radius r is centered at the position of each CA cell and the number of CA cells $v(i)$ that fall within this circle consitute the neighborhood $\mathcal{N}$ of cell i. Given this disposition of CA cells, the updating rule is easily written once an intermediate variable $\sigma(i, t)$ is computed as

$$
\sigma(i, t) = \begin{cases} 0 & \text{if } s(i, t) = 0 \text{ and } v_e(i) < m_0 + bs(i, t), \\ s(i, t) - 1 & \text{if } 0 < s(i, t) \leq k \text{ and } v_e(i) < m_0 + bs(i, t) \text{ or } s(i, t) > k, \\ n - 1 & \text{if } s(i, t) \leq k \text{ and } v_e(i) \geq m_0 + bs(i, t), \end{cases} \tag{2.2.2}
$$

where $v_e(i)$ is the number of excited cells in $\mathcal{N}$. The updating rule is

$$
s(i, t + 1) = \begin{cases} \sigma(i, t) & \text{if } \sigma(i, t) = 0, 1, n - 1, \\ [\langle \sigma(i, t) \rangle]_1 & \text{if } 1 < \sigma(i, t) < n - 1, \end{cases} \tag{2.2.3}
$$

where

$$
\langle \sigma(i) \rangle = v(i)^{-1} \sum_{j \in \mathcal{N}} \sigma(j) \tag{2.2.4}
$$

and $[\cdots]_1$ refers to the next integer. The randomization of the CA cell location on the lattice L removes the dependence of the waveform on the underlying lattice geometry; the chemical waves appear to be circular or spherical (in 3-d), so that curvature effects can be studied. In order to account for dispersion, so that the wave velocity depends on the period, it is important to include excitability of some of the refractory states. The threshold for this excitability is given phenomenologically in terms of the linear form $m_0 + bs(i, t)$. The incorporation of these features increases the complexity of the model, which now depends on the parameters r/q, n, k, b and m_0. In spite of the increased complexity, the model is computationally orders of magnitude more efficient than direct simulation of the reaction–diffusion equation and reproduces the correct qualitative forms and some quantitative features of the chemical waves.

Another version of the excitable medium CA model was studied by Gerhardt, Schuster and Tyson [43]. This model takes the phase plane structure of the propagator–

controller excitable kinectics more seriously and introduces two variables to code the state of each cell. The state of a cell is coded by a variable $s = (u, v)$ which takes the $2m$ values $\{s = (u, v) : u = 0, 1; v = 0, \ldots, m - 1\}$. As in the excitable medium models described earlier, the states are classified as quiescent $Q = (0, 0)$, refractory $R = \{s = (0, v);$ $v = 1, \ldots, m - 1\}$, or excited $E = \{s = (1, v); v = 0, \ldots, m - 1\}$. Furthermore, it is convenient to subdivide the refractory and excited states into two groups: let $R = \{R', R''\}$, where $R' = \{s = (0, v); v = 1, \ldots, k\}$ is a set of k relatively refractory states which may be excited if a sufficiently large number of neighboring cells is excited and $R'' = \{s = (0, v); v = k + 1, \ldots, m - 1\}$ is a set of $m - k - 1$ absolutely refractory states which may not be excited regardless of the states of neighboring cells. Similarly, we let $E = \{E', E''\}$, where $E' = \{s = (1, v); v = 0, \ldots, l - 1\}$ is a set of l states which are unaffected by the states of neighboring cells and $E'' = \{s = (1, v); v = l, \ldots, m - 1\}$ is a set of $m - l$ excited states which may jump prematurely to recovering states if surrounded by a sufficiently large number of quiescent or recovering states.

Given this classification of states, the CA rule is simply an elaboration of the usual excitable medium CA rule: in the absence of any interactions with neighboring cells, if the system is in the Q state it will remain there, if it is excited it will cycle through the excited and refractory states and return to the Q state. In addition, cells may be excited or de-excited depending on the states of neighboring cells. The CA rule is:

$$
s(i, t+1) = \begin{cases}
(1, 0) & \text{if } s(i, t) = (0, 0) \text{ and } v_e(i) \ge n_e, \\
(0, m - 1) & \text{if } s(i, t) = (1, m - 1), \\
(1, v') & \text{if } s(i, t) \in E' \text{ or } s(i, t) \in E''/(1, m - 1) \text{ and } v_r(i) < n_r, \\
(0, v(i, t)) & \text{if } s(i, t) \in E''/(1, m - 1) \text{ and } v_r(i) \ge n_r, \\
(1, v(i, t)) & \text{if } s(i, t) \in R' \text{ and } v_e(i) \ge n_e, \\
(0, v'') & \text{if } s(i, t) \in R'' \text{ or } s(i, t) \in R' \text{ and } v_e(i) < n_e.
\end{cases} \tag{2.2.5}
$$

In this equation, $v_r(i)$ is the number of quiescent or refractory cells in a neighborhood $\mathcal{N}$ of cell i and $v_e(i)$ is the number of excited cells in $\mathcal{N}$. The threshold numbers of quiescent or refractory and excited cells, n_r and n_e, respectively, are taken to be functions of the extent of recovery or excitation in the simulations. Selecting the neighborhood $\mathcal{N}$ to be a square of cells with sides of length $2r + 1$, the forms of n_r and n_e are:

$$
n_r(v) = n_r^0 + \left[r(2r + 1) - n_r^0 \right] \left[\frac{v - m + 1}{l - m + 1} \right],
$$

$$
n_e(v) = n_e^0 + \left[r(2r + 1) - n_e^0 \right] \frac{v}{k}. \tag{2.2.6}
$$

In general, the system may pass through the excited and refractory states at different rates, so v' and v'' are defined as follows:

$$v' = \min(v(i, t) + v_{\rm u}, m - 1), \qquad v'' = (v(i, t) - v_{\rm d}, 0), \tag{2.2.7}$$

where $v_{\rm u}$ is the rate at which v increases in the E manifold, while $v_{\rm d}$ is the rate at which v decreases in the R manifold. These features can model the dispersion of the wave velocity, as discussed above. This model has the attractive feature that the CA states are more directly related to the propagator–controller concentrations than CA models involving a single scalar set of states.

Both of the above CA rules are elaborations of the simple excitable medium automaton model designed to account for features that are absent in the original rule, in particular the dispersion of the wave velocity or curvature effects. These features are crucial for the proper description of a variety of spatio-temporal dynamics in excitable (and oscillatory) media.

Other generalizations of the excitable medium CA have been used in different contexts, e.g. to study spiral galaxy formation and parallels to chemical wave propagation processes have been noted [44].

2.3.   INHOMOGENEOUS EXCITABLE MEDIUM CA

A variant of this CA rule that introduces an additional probabilistic element has been used to model excitable medium dynamics in spatially inhomogeneous systems. We consider one such version, which has been used in a number of applications to biological systems where the inhomogeneous nature of the medium plays an important role in the wave propagation processes. Cardiac and nerve tissues are prime examples of excitable media, where the "reaction–diffusion" equation describes the coupled dynamics of the membrane potential and currents of ions such as K^+, Na^+, Ca^{++}, etc. [45].

In the heart, a complex pattern of electrochemical waves is responsible for the normal contractions of the heart muscle and disruptions of this pattern can lead to fibrillation. It is belived that fibrillation is connected to the appearance and fragmentation of spiral waves or their 3-d analogs, scroll waves, in the heart tissue [46,47]. Spiral waves can arise either because of the intrinsic inhomogeneity of the excitable medium or from the existence of phase singularities created by the excitation process. We should also remark that many of the processes that occur in excitable living tissue can be produced and studied in a controlled way in chemical excitable media, and the well-known Belousov–Zhabotinsky [48] reaction has become a testing ground for such studies [1,46,47]. In view of the variety and physiological importance of wave propagation processes in such systems, it is not surprising that a considerable amount of work has been done on CA models for these systems. In fact, as noted above, some of the earliest CA models were applied to the study of the heart [13,15].

The entire heart is a rather complicated system to model, and most studies have focussed on specific aspects of the conduction process. The wave propagation processes in the atrio-ventricular (AV) node are perhaps some of the easiest to study theoretically. The AV node is a thin rectangular piece of tissue through which the excitation in the atrium is transmitted to the ventricles [49]. Disruption in the manner in which the

electrical waves traverse the AV node can lead to abnormalities in the contractions of the ventricles. The waves that pass across the AV node may be delayed or even blocked, and it is the nature and origin of such features that is interesting to investigate.

An inhomogeneous excitable medium CA has been used to model the AV node [50,51]. The simplest version treats the AV node as a 2-d piece of tissue and the cells or blocks of cells of the tissue are assumed to lie on the nodes of an $L \times M$ rectangular lattice. Spatial inhomogeneity is introduced by making the refractory period of each cell a random variable. More specifically, the refractory period $\tau(i)$ of each cell i, independent of that of its neighbors, is obtained by taking the integer part of a random number drawn from a Gaussian distribution with mean $\bar{\tau}$ and width σ. Thus, the set of states $S(i)$ corresponding to each cell i is in general different and is given by

$$S(i) = \{Q, E, R_{\tau(i)}, R_{\tau(i)-1}, \ldots, R_1\}. \tag{2.3.1}$$

The spatial distribution of refractory periods is assigned at the initial time. Subsequent evolution of the CA occurs through the deterministic excitable medium CA rule, $\mathcal{R}_{em}$, (2.1.1), which is now a function of the specific distribution of refractory times:

$$s(i, t+1) = \begin{cases} E & \text{if } s(i, t) = Q \text{ and } s(j, t) = E, \\ R_{\tau(i)} & \text{if } s(i, t) = E, \\ R_{\tau(i)-k-1} & \text{if } s(i, t) = R_{\tau(i)-k} \ (k = 0, \ldots, \tau(i)-2), \\ Q & \text{if } s(i, t) = R_1 . \end{cases} \tag{2.3.2}$$

The evolution of the automaton has a much more complex history than that of the corresponding homogeneous CA since different parts of the medium will recover at different rates as a result of the dispersion of refractory times.

This CA model has been used to mimic the wave propagation processes across the AV node by periodically exciting the top row of the rectangular lattice and observing the timing and nature of the waves of excitation that exit from the bottom of the array. Absorbing boundary conditions are assumed at the sides of the lattice. More specifically, the simulations are carried out in the following way: a random distribution of refractory times is first assigned to the lattice. Given that the system is in the quiescent state, at $t = 0$, with probability p each site in the first row of M sites is perturbed to the excited state E. The perturbation is periodically applied every T time steps to the first row of sites, thereby simulating the periodic impingement of waves of excitation from the atrium on the AV node. If a site in the first row is in a refractory state when the excitation is applied, it is not excited, so that the effective excitation probability may be less than p for the subsequent stimuli. Statistically significant quantities are obtained by averaging over different realizations of the excitation process, as well as over different realizations of the distribution of refractory times on the lattice. It is in such lengthy averaging calculations that the utility of the automaton is manifested.

The model exhibits the same characteristic wave propagation features as the real AV node. The conduction is considered to be normal if the excitation takes L time steps to traverse the array with length L. Depending on the period of excitation T, the average refractory period $\bar{\tau}$ and its dispersion σ, different types of wave propagation are observed. For every excitation, a wave may traverse the array but experience a delay; in addition, various types of blocks of the form $M:N$ are possible, where for every M stimuli, N waves are observed to exit from the bottom of the array. Other phenomena with physiological analogs are also observed; for example, the Wenkebach process, where waves are progressively delayed by longer and longer periods until a block results. These data are summarized in the phase diagram of fig. 6, which is a plot of the type of wave propagation
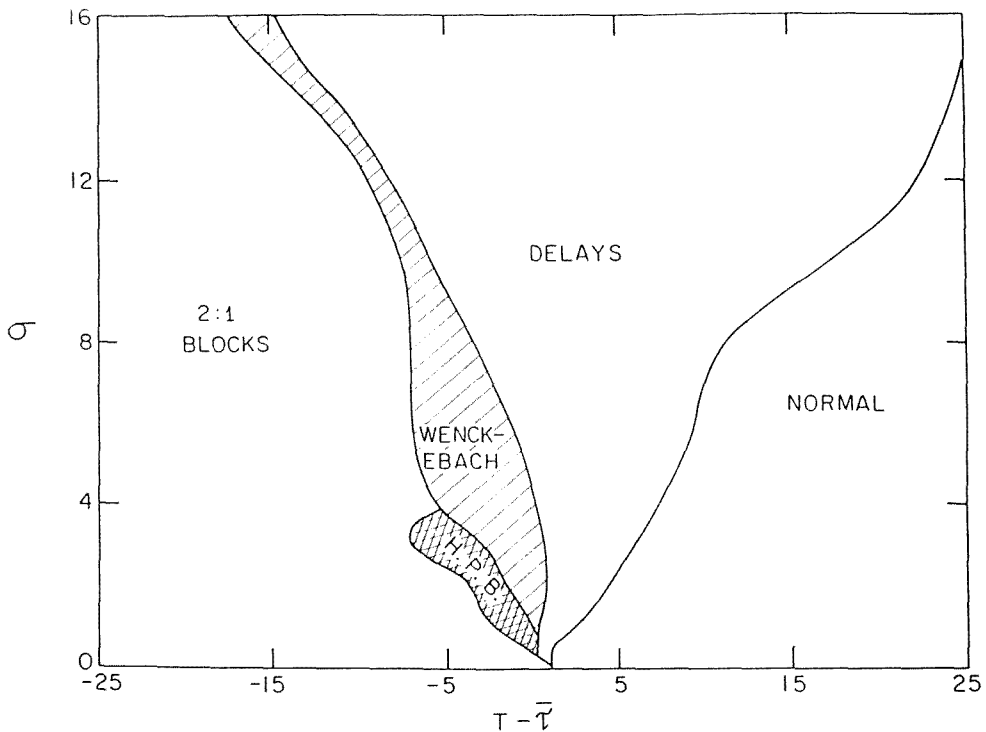

Fig. 6. Phase diagram showing the different types of wave propagation processes in the AV node model as a function of $(T - \bar{\tau})$ and σ.

process versus the quantity $(T - \bar{\tau})$ as the abscissa and σ as the ordinate. The figure illustrates the rich variety of wave processes that the CA can produce. In addition, the details of the fragmentation of the wave front as it moves across the AV node can be studied. In certain parameter regions the formation of circular fronts is observed which arise from the inhomogeneous nature of the medium, and an example of the evolution of such a wave is shown in fig. 7. Quantitative aspects of some of these phenomena have
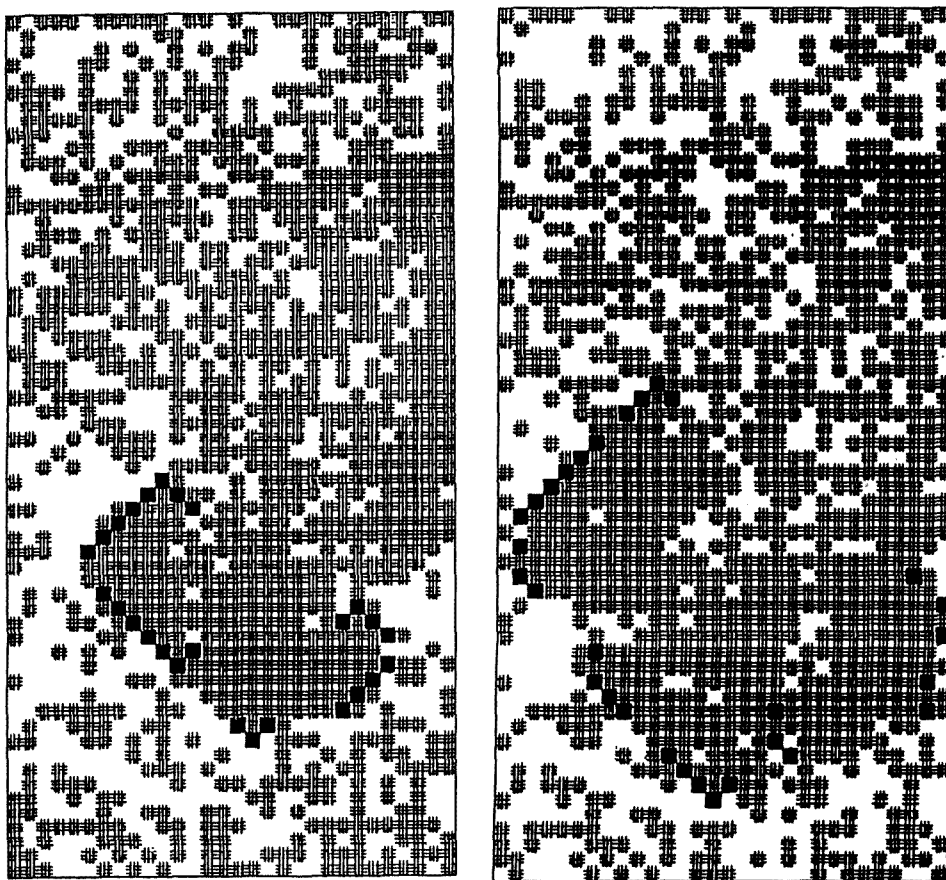
Fig. 7. An example of circular wave formation in the
AV node using the inhomogeneous excitable CA model.

also been described in the context of the CA model [51]. Naturally, this simple model
suffers from some of the defects of the simple excitable medium CA, but dispersion
and curvature effects can be included using the generalizations described earlier in
section 2.2.

Inhomogeneities can also play a crucial role in the dynamics of excitable chemical
systems. Recently, experiments have been performed by Maselko, Reckley and Showalter
on another type of inhomogeneous excitable system: the Belousov–Zhabotinsky reaction
carried out on a random array of beads [52]. In this case, irregular packing of the spheres
containing the immobilized catalyst consistutes an inhomogeneous substrate for the
pattern formation process. Interesting spiral wave formation and break-up dynamics are
observed as a function of initial reagent concentrations. Excitable medium CA models
have been constructed to study these processes [53]. The five-state excitable medium CA
model used in this study incorporates two principal features. Random initial seeding with
both excited and refractory states gives rise to a collection of spiral centers as described

earlier, and inhomogeneity in the medium is taken into account by modifying the CA rule in certain local spatial regions so that both quiescent and refractory states may be excited by neighboring excited cells. Such a simple model can account for some of the features of the complicated wave dynamics seen in the experiments.

The preceding sections have given only a brief outline of the variety of wave propagation processes that occur in excitable media. Since the focus was intentionally restricted to the application of discrete models to such systems, no exhaustive review of phenomena like the dynamics of waves in media with obstacles, curvature and dispersion effects on wave dynamics in two and three dimensions, or spiral core dynamics was attempted. New experimental techniques such as the use of the continuously fed unstirred reactor [54], the gel reactor [55], and the Couette reactor [56] have opened up the possibility of studying chemical wave structure and dynamics in excitable and other media with greater control and detail than has hitherto been possible. For example, such reactors have been used experimentally to observe [55] Turing bifurcations [57] and spiral wave dynamics [27], and have prompted a number of theoretical studies of pattern formation processes for these experimental conditions [58]. CA models can contribute to the interpretation of such experiments, and most likely there will be a considerable amount of activity in this direction in the future.

2.4.   REACTIVE CA MODELS

Cellular automaton models have been used to describe other types of chemically reacting systems, and we mention below a few examples in order to illustrate how such models are constructed.

A variation of the generalized excitable medium CA rule has been used to construct cellular automaton models for the surface oxidation of CO_2 catalyzed by Pd crystallites in a zeolite matrix [59–61]. The "hodge-podge" machine [61] was devised to investigate this problem and illustrates the more complex variations of this type of model. The CA model for this system considers states analogous to the $\{Q, R_1, R_2, \ldots R_l, E\}$ states defined above (called "healthy, infected and ill"), together with a more complex updating rule. Coding the elements in the set S as $S = \{Q, R_1, R_2, \ldots, R_l, E\} = \{0, 1, 2, \ldots, l+1\}$, the CA rule takes the form:

$$s(i, t+1) = \begin{cases} \left[\dfrac{v_e(i)}{k_1} \right] + \left[\dfrac{v_r(i)}{k_2} \right], & \text{for } s(i,t) = 0, \\[2ex] \min \left\{ \left[\dfrac{T(i)}{v_r(i,t)} \right] + \bar{v}, l+1 \right\}, & \text{for } s(i,t) \in R, \\[2ex] 0, & \text{for } s(i,t) = l+1. \end{cases} \qquad (2.4.1)$$

In this equation, $v_e(i)$ is the number of neighbors of i that are in the state E, $v_r(i)$ is the number of neighbors that are in any of the R states, and $T(i)$ stands for the sum

$$T(i) = \sum_{j \in \mathcal{N}} s(j, t), \quad s(j, t) \in R. \qquad (2.4.2)$$

The bracket [$\cdots$] stands for the integer part of its argument and k_1, k_2 and $\bar{v}$ are integers. The integer $\bar{v}$ determines how rapidly the system runs through the R states. The spatial patterns produced by this CA are quite similar to those observed not only in the CO_2 oxidation problem, but also to those of the BZ reaction.

A simple CA model for heterogeneous catalysis has been studied by Chopard and Droz [62]. A gas mixture composed of atomic A and diatomic B_2 species is supposed to be in contact with a surface. The surface is imagined to be divided into cells, each of which can adsorb one *atom*. The B_2 molecule must dissociate before it can be adsorbed; thus, if a B_2 molecule approaches an empty cell it will dissociate and be adsorbed only if there is an empty cell adjacent to the original cell. Finally, if two neighboring cells are occupied by different species they may react to form a product which is desorbed. The chemical mechanism corresponding to the above is

$$A \rightarrow A(ads), \quad B_2 \rightarrow 2B(ads),$$

$$A(ads) + B(ads) \rightarrow AB(desorb). \tag{2.4.3}$$

The gas above the surface is continuously renewed and the adsorption probabilities are assumed to be proportional to the mole fractions of the given species (x_A for A and $1 - x_A$ for B_2).

A simple CA rule that describes such kinetics can be constructed as follows. The cells of the surface are the CA cells; each cell can exist in any of four states: $S = \{0, A, B, C\}$. Here, 0 is the empty cell, A and B are states of cells occupied by A and B species, respectively, while the state C accounts for the conditional occupancy by B: it will become 0 or B, depending on the states of its neighbors. Using these simple physical ideas the following CA model can be written to describe the dynamical evolution of the system:

$$s(i, t+1) = \begin{cases} 0 & \text{if } s(i,t) = A \text{ and } s(j,t) = B \text{ or} \\ & \quad s(i,t) = B \quad \text{and } s(j,t) = A \text{ or} \\ & \quad s(i,t) = C \quad \text{and } s(j,t) = C; \\ A & \text{if } s(i,t) = A \text{ and } s(j,t) \neq B \text{ or} \\ & \quad \text{with prob } x_A \text{ if } s(i,t) = 0; \\ B & \text{if } s(i,t) = B \text{ and } s(j,t) \neq A \text{ or} \\ & \quad s(i,t) = C \quad \text{and } s(j,t) = C; \\ C & \text{with prob } 1 - x_A \text{ if } s(i,t) = 0. \end{cases} \tag{2.4.4}$$

This crude model can show very interesting kinetics and in fact exhibits a nonequilibrium surface phase transition whose critical properties can be studied.

There is a large variety of models that can be constructed along similar lines; for example, CA models have been used to study diffusion controlled reactions [63,64] and reversible versions of the GH models have been studied in some detail [65]. Additional references to such work can be found in the above-mentioned papers, and we shall not provide other examples here.

3.   Coupled map lattices

Coupled map lattices (CML) constitute a general class of dynamical systems where space and time are discrete but the dynamical variables take on a continuum of values [66–68]. Like the cellular automaton models discussed in the previous section, space is discretized by placing the system on a d-dimensional lattice. In a coupled map model, the CA updating rule is replaced by a nonlinear function that describes both the local dynamics of each cell as well as the coupling among cells. If we let $c(i, t)$ represent a vector of local dynamical variables at discrete time t (these are chemical concentrations in our case), the general form of the evolution equation for a coupled map lattice is

$$c(i, t + 1) = f(c(i, t)) + C(c(j, t)), \tag{3.1}$$

where i again labels lattice sites or cells and $j \in \mathcal{N}$ labels cells neighboring i. The function f specifies the local dynamics of a cell, while C accounts for the coupling of cell i to its neighbors.

Most often, the coupling term C is taken to be a discrete version of the Laplacian, either in its backward difference form so that

$$c(i, t+1) = f\big(c(i, t)\big) + \gamma \sum_{j \in \mathcal{N}} \big(c(j, t) - c(i, t)\big), \tag{3.2}$$

or in its forward difference form so that

$$c(i, t+1) = f(c(i, t)) + \gamma \sum_{j \in \mathcal{N}} \big(f(c(j, t)) - f(c(i, t))\big), \tag{3.3}$$

but other forms are possible. In these equations, γ is a matrix of coupling coefficients. Even the one-dimensional versions of these equations can yield a wide range of interesting dynamical behavior; for example, spatio-temporal versions of period doubling and intermittency. These aspects of coupled map lattices will not be recounted here since reviews exist [69]; however, in keeping with the topic of this review, the utility of such models for the study of pattern formation processes in spatially distributed chemically reacting systems will be described.

Coupled map lattices are dynamical systems in their own right and need not be regarded as approximations to other dynamical models like the partial differential equations used to model fluid flow or reaction–diffusion systems. However, in some circumstances it is clear that a partial differential equation such as the reaction–diffusion equation provides a good description of a physical system, and in this case it is useful to attempt to reproduce the major features of the solution structure with a simpler discrete model. The aim is to construct a discrete model that is in the same "universality class" as the original reaction–diffusion equation without slavishly reproducing all details of the dynamics. We shall describe such constructions below for several specific types of chemically reacting systems.

3.1. BISTABLE SYSTEMS

In contrast to reactions occurring near equilibrium, nonequilibrium chemical systems may evolve to more than one stationary state depending on the initial concentrations. There are many examples of real systems that show this kind of behavior [70], but it is convenient to describe the phenomena with reference to an abstract chemical reaction scheme devised by Schlögl [71]. The Schlögl reaction consists of the following elementary steps:

$$C \xrightarrow{k_0} X + B, \qquad X + B \xrightarrow{k_1} C,$$

$$2X + A \xrightarrow{k_2} 3X, \quad 3X \xrightarrow{k_3} 2X + A. \tag{3.1.1}$$

The macroscopic rate law for the concentration x of the X species is

$$\frac{dx}{dt} = -k_3 x^3 + k_2 a x^2 - k_1 b x + k_0 c, \tag{3.1.2}$$

where a, b and c are the concentrations of A, B and C, respectively. The system is maintained away from equilibrium by fixing the concentrations of A, B and C, so they may be incorporated into the definitions of the rate constants k_i. In order to describe the solution structure of this equation, it is convenient to scale the time ($t \rightarrow k_3 t$) and introduce an order parameter field $\phi = x - k_2 a/3k_3$ so that the rate law takes the simpler form

$$\frac{d\phi}{dt} = -\phi^3 + \varepsilon\phi + \mu = -\frac{dV(\phi)}{d\phi}, \tag{3.1.3}$$

where

$$\varepsilon = 3\left(\frac{k_2 a}{3k_3}\right)^2 - \frac{k_1 b}{k_3}, \quad \mu = 2\left(\frac{k_2 a}{3k_3}\right)^3 - \frac{k_1 k_2 ab}{3k_3^2} + \frac{k_0 c}{k_3}, \tag{3.1.4}$$

and $V(\phi)$ is a quartic potential function defined by (3.1.3). The steady states of the system are given by the solutions of $-\phi^3 + \varepsilon\phi + \mu = 0$ so that for certain values of ε and μ there are three real roots, two of which are temporally stable and the other unstable. The solution structure in the $\varepsilon\mu$-plane is shown in fig. 8, where the physically relevant region of bistability is shaded. States along the dashed line within the shaded region are equivalent in that they have the same stability, with order parameter values differing only by sign, $\phi = \pm\sqrt{\varepsilon}$. Off this $\mu = 0$ line the two coexisting states are inequivalent, being characterized by different relaxation rates for perturbations about these states.

A real chemical system which is well approximated by cubic kinetics for a single intermediate species is the iodate-arsenous acid system [72]. While the actual chemical mechanism [73] is much more complicated than the Schlögl mechanism (3.1.1), under suitable conditions corresponding to either excess iodate or arsenous acid, the chemical
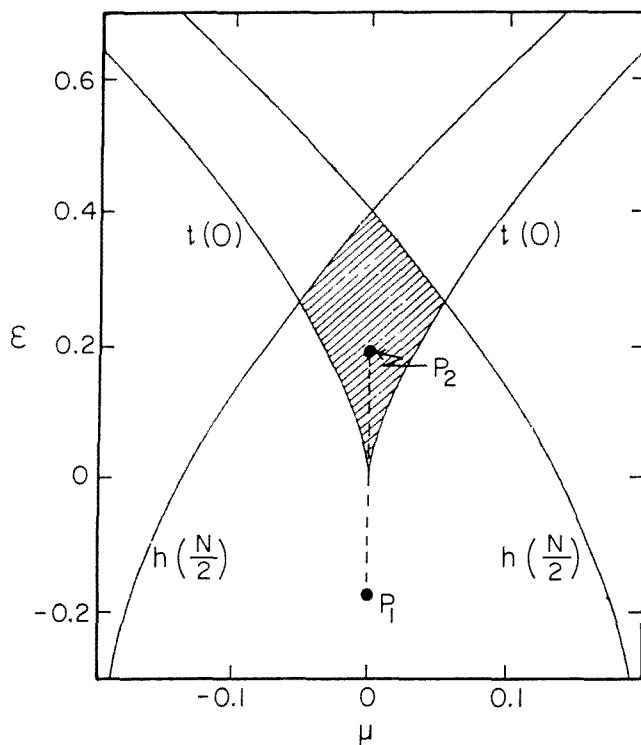
Fig. 8. Bifurcation diagram for the Schlögl model CML showing tangent
and subharmonic boundaries with the physically relevant region of bistability
shaded. The dashed line indicates the critical quench path. The bifurcation
boundary for the continuous Schlögl model is the tangent boundary.

rate law is a cubic polynomial. For example, under conditions of excess arsenous acid,
the net reaction is

$$IO_3^- + 3H_3AsO_3 \rightleftarrows I^- + 3H_3AsO_4$$
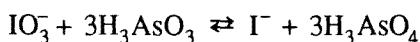
and the rate law for the concentration of the iodide ion $x = [I^-]$ is

$$\frac{dx}{dt} = x(k_A + k_B x)(y_0 - x),\tag{3.1.5}$$

where $y_0 = [IO_3^-]_0$, the initial value of the iodate ion concentration, while k_A and k_B are
effective rate constants that depend on the hydrogen ion concentration. Typical values
for these parameters may be found in Saul and Showalter [72]. For our purpose, it is
sufficient to note that with suitable rescaling of concentration and time variables, (3.1.5)
can be cast into the form of (3.1.2). However, there are a number of unusual features.
For parameter values corresponding to the standard experimental conditions, one of the

steady states of (3.1.5) is unphysical since it corresponds to negative concentrations. Also, experimentally the system may be prepared at the unstable steady state, so a number of interesting features associated with evolution from the unstable state may be investigated. These include consumption fronts where the chemical medium is converted from the unstable state to the stable state [72].

The reaction–diffusion equation corresponding to (3.1.3) has the form of the time-dependent Ginzburg–Landau (TDGL) equation for a system with a non-conserved order parameter field:

$$\frac{\partial \phi(r, t)}{\partial t} = -\phi^3(r, t) + \varepsilon \phi(r, t) + \mu + D\nabla^2 \phi(r, t). \tag{3.1.6}$$

The qualitative features of the dynamics of this equation are well known [74]. Consider a "critical quench" where the system parameters are suddenly changed along the line $\mu = 0$ from those corresponding to point P_1 (cf. fig. 8), where the potential V has a single minimum at $\phi = 0$ to point P_2 within the bistable region where V has two minima at $\phi = \pm\sqrt{\varepsilon}$ separated by a maximum at $f = 0$. As a result of fluctuations either in the dynamics or in the initial state, the system will segregate into domains of the two spatially homogeneous stable states. The average order parameter in an infinite system will be zero, but the system will generate order on arbitrary length scales. Finite systems will evolve to one or the other of the stable states, but the order parameter averaged over realizations of the initial state corresponding to small inhomogeneous fluctuations about the unstable state will be zero. After an initial stage with complex dynamics during which well-defined boundaries between the coexisting stable states are established, the longer time evolution of the system is characterized by domain growth with simple features. This late stage growth region was discussed by Allen and Cahn [75] and is dominated by the dynamics of the curved surfaces separating the domains. If $R(t)$ is the characteristic size of a domain at time t, then the curvature of the domain boundary gives rise to a growth law $R(t) \sim t^{1/2}$. It is convenient to quantitatively characterize the non-equilibrium dynamics of the system in terms of the correlation function $C(r, t)$ defined by

$$C(r, t) = \mathcal{V}^{-1} \int_{\mathcal{V}} dr' \langle \phi(r', t) \phi(r + r', t) \rangle, \tag{3.1.7}$$

where $\mathcal{V}$ is the volume of the system and the angle brackets signify an average over realizations of the growth process. For systems with translational invariance, this is a function of the scalar distance r. The dynamic structure factor is the Fourier transform of the correlation function:

$$S(k, t) = \int dr\, e^{ik \cdot r} C(r, t). \tag{3.1.8}$$

If one makes the assumption that the only relevant length in the system is the domain size and assumes the domain size growth law given above, then the dynamic structure

factor satisfies the scaling relation $S(k, t) \sim t \, \mathcal{F}(kt^{1/2})$ and thus possesses simple scaling properties.

Off the line $\mu = 0$, the states are no longer equivalent and growth occurs by a nucleation process. For example, if the system is initially prepared in the less-stable state and seeded with nuclei of the more-stable state, then the nuclei will grow provided they are larger than some critical size and the system will evolve to the more-stable state. In general, the morphology of this growth process differs from that along the critical $\mu = 0$ line. From the above description of the dynamics, it is clear that the domain curvature plays a central role in the dynamics and morphology of the inhomogeneous states; thus, it is essential that this feature be correctly described in any discrete model for these phenomena.

The simplest CML results from an Euler-like discretization of the TDGL model. Letting τ and q be the time and space increments, we have

$$\phi(i, t+1) = -\phi^3(i, t) + (\varepsilon + 1)\phi(i, t) + \mu + \gamma \sum_{j \in \mathcal{K}} \left[\phi(j, t) - \phi(i, t) \right], \qquad (3.1.9)$$

where ϕ has been scaled as $\phi \rightarrow \sqrt{\tau}\phi$ and t is measured in units of τ. The parameters in (3.1.9) are related to those in the TDGL equation by the transformations (we use the same symbols to avoid proliferation of notation) $\varepsilon \rightarrow \tau\varepsilon$, $\mu \rightarrow \tau^{3/2}\mu$ and $\gamma = D\tau/q^2$. Thus, the bifurcation structure can be studied as a function of ε, μ and γ. It is clear that for small enough τ and q, the solutions of (3.1.9) approximate those of (3.1.6). However, many aspects of the bifurcation structure may be studied with a coarse discretization grid. The map model (3.1.9) then consists of a lattice of coupled cubic maps. As such, it will generate a much richer bifurcation structure than the original TDGL model [76]. However, provided the bifurcation parameters ε, μ and γ are suitably selected, the coupled map lattice will exhibit spatio-temporal phase separation behavior like that of the reaction–diffusion equation. It is simple to study the stability of the homogeneous steady states of (3.1.9). These steady states are given by the solutions of $-\phi^3 + \varepsilon\phi + \mu = 0$ and are identical to those discussed earlier with a suitable reinterpretation of the parameters. Temporal stability of these states is most conveniently studied by considering the spatial Fourier transform of the linearized version of (3.1.9). Depending on the slope of the linearized Fourier transformed map, two sets of bifurcation boundaries are obtained: for slope $+1$ there are tangent boundaries,

$$t(k) : \mu = \pm \left[-2\varepsilon + w(k) \right] \left[(\varepsilon + w(k)) \right]^{1/2}, \qquad (3.1.10)$$

while for slope -1 there are subharmonic boundaries,

$$h(k) : \mu = \pm \left[2(1 - \varepsilon) + w(k) \right] \left[\varepsilon + 2 + w(k) \right]^{1/2}. \qquad (3.1.11)$$

These boundaries are clearly functions of the wave vector k and the diffusive coupling strength through $w(k)$, which is defined as

$$w(k) = 4\gamma\{\cos[\pi(k_1 + k_2)/N]\cos[\pi(k_1 - k_2)/N] - 1\}, \tag{3.1.12}$$

for an $N \times N$ array of maps on a square lattice with periodic boundary conditions. Here, the wave vector $k = (k_1, k_2)$. For $\gamma > 0$, the relevant tangent boundary (that corresponding to the most unstable mode) has $k = (0, 0)$ and is just that sketched in fig. 8 for the continuous space and time equation (3.1.6). The boundary labeled $h(N/2)$ in this figure is the relevant subharmonic boundary for which $k = (N/2, N/2)$. This mode corresponds to a "checkerboard" pattern inhomogeneous state and is a feature of the coupled map model. Thus, within this bifurcation boundary the phase separation phenomena exhibited by the coupled cubic map lattice will mimic those of the TDGL model. Outside this boundary, the coupled map lattice displays a variety of secondary bifurcations, giving rise to interesting spatio-temporal structures which are different from those of the TDGL model but have parallels in real physical phenomena. Such features have been extensively studied for coupled quadratic and other maps [69]. Here, however, we focus on the spatio-temporal dynamics that are like those of the Schlögl reaction–diffusion system or, more generally, the TDGL model.

A coupled map simulation of the critical quench can be carried out easily, and fig. 9 shows the results of such a calculation. The initial condition corresponding to a critical quench was constructed by superimposing small amplitude fluctuations on the homogeneous system with order parameter equal to that of the unstable state, $\phi = 0$. The subsequent evolution is deterministic. Sharp domains are established within a few tens of time steps, after which the domain growth is governed by domain wall curvature effects. The scaling relations for the dynamic structure factor have been shown to be valid for the CML in this long time regime. In addition, a CML model of the iodate-arsenous acid system has been constructed to study the one-way evolution from the unstable state [77]. The map model simulations suggest a number of features that can be experimentally studied since it is easy to prepare the system in the unstable state [72]. Thus, the map model can be used to explore a range of phenomena in such systems, and these studies may be extended to include nucleation and growth processes where the order parameter is conserved [78]. In this latter case, the status of the scaling relations is the subject of some controversy which the CML simulations may help to resolve. As for the spiral wave curvature effects discussed in section 2, the domain evolution in these bistable systems is governed by the curvature of the chemical waves. Hence, it is essential that the discrete model correctly describes such effects. The simple cubic CML has been demonstrated to do so.

Before leaving the topic of bistable states, it is interesting to enquire a little more deeply into the nature of the interface that separates the domains of stable states in these discrete systems, since such interfaces or defects often govern the system dynamics [76]. The simplest case to consider is that of a planar interface for which a one-dimensional coupled map lattice suffices. The stationary solutions of (3.1.9) for one dimension are given by

$$-\phi^3(i) + \varepsilon\phi(i) + \mu + \gamma[\phi(i+1) + \phi(i-1) - 2\phi(i)] = 0, \tag{3.1.13}$$
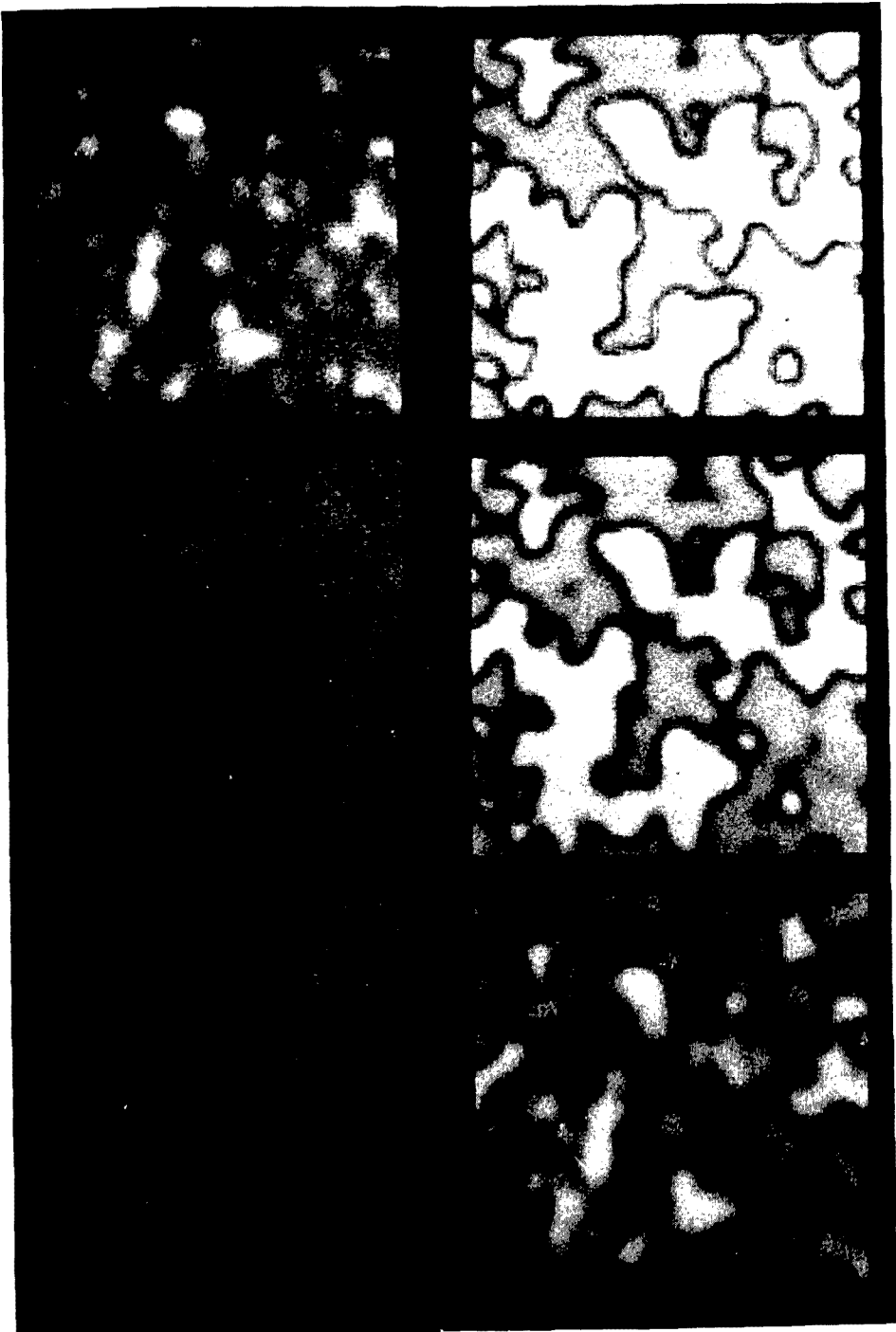
Fig. 9. CML simulation of a critical quench showing domain formation and growth from the unstable state. System parameters are $\varepsilon = 0.2$, $\mu = 0$ and $\gamma = 0.1$. Time increases from left to right and top to bottom in the six panels.

which may be written as a two-dimensional conservative map by letting $\psi(i) = \phi(i-1)$:

$$\phi(i+1) = -\gamma^{-1}[-\phi^3(i) + \varepsilon\phi(i) + \mu] + 2\phi(i) - \psi(i),$$

$$\psi(i+1) = \phi(i). \tag{3.1.14}$$

The solutions of this two-dimensional mapping give all the stationary inhomogeneous solutions of the 1-d coupled map lattice. The solution structure in the $\phi\psi$-plane for $\mu = 0$ obtained by iterating a random distribution of points in the plane is shown in fig. 10. The hyperbolic character of the two temporally stable fixed points $\phi_{\pm} = \pm\sqrt{\varepsilon}$ is
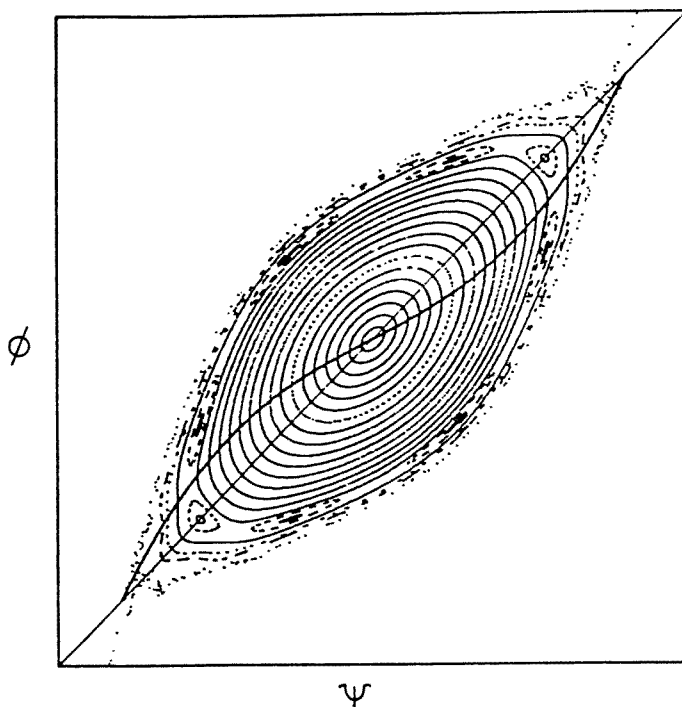

Fig. 10. Discrete stationary inhomogeneous solution structure obtained by iteration of the conservative map (3.1.14). System parameters are $\varepsilon = 0.15$, $\mu = 0$ and $\gamma = 0.15$. The solid line is one of the symmetry curves for the conservative map (cf. ref. [76]).

evident from the figure, as is the elliptic character of the temporally unstable fixed point at $\phi = 0$. The conservative mapping (3.1.14) clearly shows regions of regular and chaotic behavior typical of nonlinear conservative maps.

The stationary planar interfacial profile may be discussed in terms of this map. Consider an infinite 1-d system (coordinate z) with boundary conditions on the order

parameter $\phi(z \to +\infty) = \phi_\pm$. The stationary planar interface of the TDGL model is the trajectory of

$$D \nabla^2 \phi(z) - \phi^3(z) + \varepsilon \phi(z) = 0, \tag{3.1.15}$$

with the above boundary conditions on $\phi(z)$. The solution is well known and is the usual hyperbolic tangent profile [71,79,80]

$$\phi(z) = -\phi_+ \tanh\left(\left(\frac{\varepsilon}{2D}\right)^{1/2} z\right), \tag{3.1.16}$$

and the corresponding trajectory is just the saddle connection between the two hyperbolic fixed points. The saddle connection is destroyed in the coupled map model. Instead, the stable $W_s^\pm$ and unstable $W_u^\pm$ manifolds emanating from the $\phi_\pm$ fixed points intersect in an infinite number of points, and the points in the discrete interfacial profile are contained in the intersection $W_s^+ \cap W_u^-$ or $W_s^- \cap W_u^+$. Not all points in these intersection sets belong to the stable profile. The closed invariant curves of (3.1.14) have two symmetry properties: they possess a symmetry with respect to the bisectrix $\phi = \psi$, and also a symmetry with respect to $\phi = -\psi$. This leads to two discrete orbits connecting the hyperbolic points:

$$-\phi(-i) = \phi(i+1), \quad i \geq 0 \tag{3.1.17}$$

and

$$-\phi(-i) = \phi(i), \qquad i \geq 0, \tag{3.1.18}$$

where we have assumed that the 1-d lattice sites are labeled from $i = -\infty$ to $i = +\infty$. The intersection points satisfying (3.1.17) and (3.1.18) correspond to alternative intersections of the stable and unstable manifolds. The manifolds may be generated numerically by iterating a set of points slightly displaced along the eigenvectors corresponding to the map linearized about the two hyperbolic fixed points. The corresponding eigenvalues are $\lambda_\pm = (1 + \varepsilon/\gamma) \pm [\varepsilon/\gamma(2 + \varepsilon/\gamma)]^{1/2}$ and the eigenvectors are $\hat{e}_\pm^T = (\lambda_\pm, 1)$, where T stands for the transpose. Numerical construction of the manifolds in this way yields fig. 11. In this figure, the points corresponding to the two types of intersections are labeled by squares (3.1.17) and crosses (3.1.18). The intersections corresponding to (3.1.18) do not lie on the stable interfacial profile. This set of intersection points contains the unstable fixed point $\phi = 0$ so that any small perturbation will cause the system to evolve to the set of points given by (3.1.17). The numerically generated profile does indeed satisfy (3.1.17). A similar analysis has been carried out for a CML where the order parameter is conserved [81]. The corresponding spatial map is four dimensional and new features arise.

    The problem of the discrete interface has many parallels in other problems in physics, like pinning of charge density waves and the commensurate–incommensurate
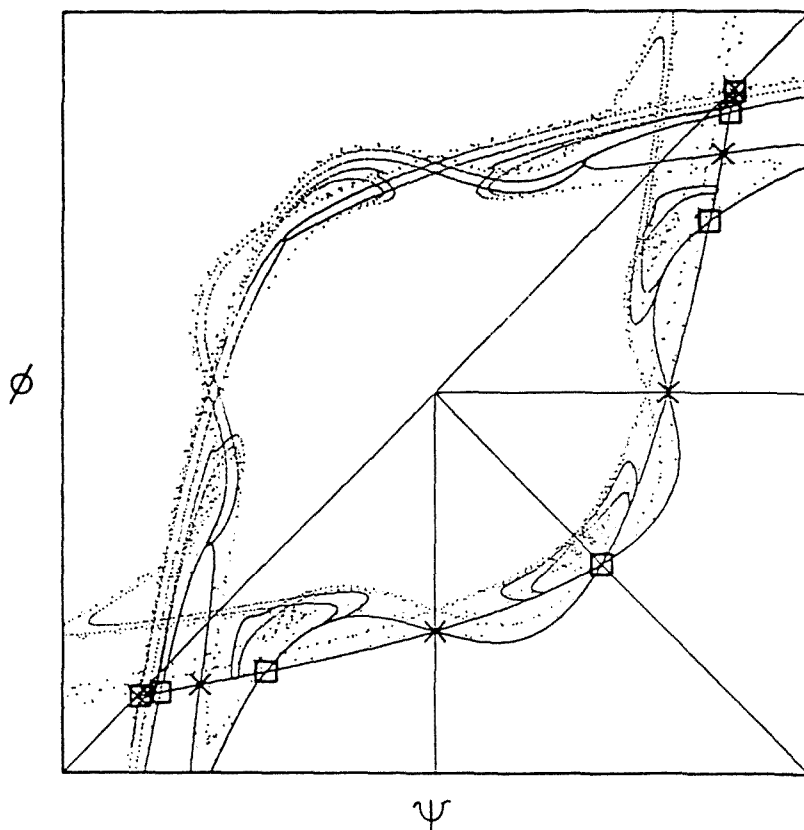
Fig. 11. Stable and unstable manifolds of the hyperbolic fixed points with squares and crosses denoting the intersections satisfying (3.1.17) and (3.1.18), respectively. The system parameters are $\varepsilon = 0.3$, $\mu = 0.0$ and $\gamma = 0.15$.

phase transition, where a similar analysis has been applied [82]. The extension of these considerations to two and higher dimensions is an interesting and challenging task since the geometry of the interface may be complicated and the discrete analog of curvature effects comes into play.

The CML corresponding to the TDGL equation was obtained by a simple Euler-like discretization and care was used to select the relevant parameter values for the study of phase separation. This is not the only way to construct a CML for this system. Oono and Puri [83] have described an alternative way to construct a CML that is convenient if attention is restricted to the case $\mu = 0$ corresponding to a critical quench. Consider (3.1.3) for $\mu = 0$; this equation may be directly integrated over an arbitrary time interval τ to yield the map

$$\phi(t+1) = \frac{\sqrt{\varepsilon}\phi(t)}{[\varepsilon v + \phi^2(t)(1-v)]^{1/2}} \equiv f(\phi(t)), \qquad (3.1.19)$$

where $v = \exp(-2\varepsilon)$, t has been measured in units of τ and ϕ has been suitably re-scaled. The function f may now be used in (3.2) or (3.3) in order to construct the coupled map lattice. The map (3.1.19) has the same fixed points as (3.1.3) and is a monotonic function of ϕ, and thus does not exhibit the subharmonic bifurcation of (3.1.9). This type of model has been used to explore phase separation phenomena for both conserved and non-conserved order parameter systems [84]. We shall continue the discussion of CML models of this type for oscillatory systems below. Both the map model (3.1.9) with suitably chosen parameter values and the map model constructed from (3.1.19) with (3.2) or (3.3) yield physically accurate descriptions of phase separation processes and chemical wave propagation in these types of bistable systems.

3.2.   OSCILLATORY SYSTEMS

The prototypical equation for the description of the onset of oscillations in a spatially distributed medium is the complex Ginzburg–Landau equation for the *complex* order parameter field $\chi(r, t)$ [4,5]:

$$\frac{\partial \chi(r, t)}{\partial t} = -(1 + i\alpha) |\chi(r, t)|^2 \chi(r, t) + \varepsilon \chi(r, t) + (1 + i\beta)\nabla^2 \chi(r, t). \quad (3.2.1)$$

This equation has the same structural form as the TDGL equation (3.1.6) for $\mu = 0$ but with complex coefficients for the cubic and diffusion terms. Consider the spatially homogeneous case for which the diffusive coupling term vanishes. In this case, (3.2.1) is equivalent to the pair of real equations

$$\frac{dA(t)}{dt} = -A^3(t) + \varepsilon A(t), \qquad (3.2.2a)$$

$$\frac{d\theta(t)}{dt} = -\alpha A^2(t), \qquad (3.2.2b)$$

letting $\chi = A \exp i\theta$. For $\varepsilon < 0$, the system admits a stable steady-state solution at $A = 0$, while for $\varepsilon \geq 0$ (3.2.2a) admits solutions $A = \pm \sqrt{\varepsilon}$, giving rise to oscillations with period $T_0 = 2\pi/\alpha\varepsilon$.

The complex Ginzburg–Landau equation is generic in the sense that any two-variable reaction–diffusion equation can be reduced to this normal form in the vicinity of the Hopf bifurcation point. A well-known two-variable model is the Brusselator [85], and we shall devote a considerable amount of space to a description of its dynamics and indicate how a Brusselator CML can be constructed. The reduction of the Brusselator (near the Hopf bifurcation point) to the complex Ginzburg–Landau model has been carried out explicitly by Kuramoto [5]. The Brusselator reaction mechanism is [85]:

$$A \overset{k_1}{\to} U,$$

$$B + U \overset{k_2}{\to} V + D,$$

$$2U + V \overset{k_3}{\to} 3U,$$

$$U \overset{k_4}{\to} E, \tag{3.2.3}$$

with reaction–diffusion equation (in scaled form)

$$\frac{\partial u}{\partial t} = a - (b+1)u + u^2 v + D_x \nabla^2 u,$$

$$\frac{\partial v}{\partial t} = bu - u^2 v + D_y \nabla^2 v, \tag{3.2.4}$$

where the lower case variables are concentrations corresponding to the upper case species. This equation is of course of the form of (1.1) if we let $c^T = (u, v)$, where T stands for the transpose:

$$\frac{\partial c}{\partial t} = R(c) + D \cdot \nabla^2 c, \tag{3.2.5}$$

where the specific form of R can be found by comparison with (3.2.4). The spatially homogeneous Brusselator possesses a stable steady state at $(u, v) = (a, b/a)$ for $b < a^2 + 1 = b^*$ which undergoes a Hopf bifurcation to a globally attracting limit cycle for $b \geq b^*$ [86]. Away from this bifurcation point, the Brusselator oscillations take on the character of relaxation oscillations, and a new time scale in addition to the period of the limit cycle is introduced into the problem.

Below we describe coupled map lattices that mimic the behavior of both the complex Ginzburg–Landau model and the Brusselator in the relaxation oscillation regime, and describe how phenomena like phase and amplitude turbulence as well as random distributions of spiral waves and target patterns arise in these systems.

A CML for the complex Ginzburg–Landau equation can be constructed using the method [83] outlined in the previous section [87]. Equation (3.2.2a) is identical to (3.1.3) for $\mu = 0$ with a change of symbols so its time integral is given by (3.1.19):

$$A(t+1) = \frac{\sqrt{\varepsilon} A(t)}{[\varepsilon v + A^2(t)(1 - v)]^{1/2}}. \tag{3.2.6}$$

Using (3.2.6), eq. (3.2.2b) may be integrated to yield

$$\theta(t+1) = \theta(t) + \frac{\alpha}{2} \ln [1 + A(t)^2 (1 - v)/\varepsilon v]. \tag{3.2.7}$$

This pair of equations defines a vector-valued map for the pair of variables (A, θ). Alternatively, we may define $u = \text{Re}(\chi)$ and $v = \text{Im}(\chi)$ and let $c^T = (u, v)$ and thus recast (3.2.6) and (3.2.7) as a map $G(c)$. The complex Ginzburg–Landau CML may then be obtained by letting $f(c) = G(c)$ in (3.2) or (3.3) [88]. A map [87] similar to the one above has been used to explore the onset of defect-mediated turbulence in such systems [89]. In the sequel, we shall also describe its application to the spatio-temporal dynamics in a randomly perturbed oscillatory medium.

An analogous procedure may be used to construct a CML for the Brusselator, but it is somewhat more involved since the reaction–diffusion equation cannot be integrated analytically [90]. However, it can easily be integrated numerically and thus it is possible to construct a Brusselator CML that behaves, in a gross sense, like the Brusselator reaction–diffusion system. More formally, we suppose that the chemical rate law for the Brusselator may be integrated over a time interval τ to yield a map $B(c)$. Measuring time in units of τ, we have

$$c(t+1) = \int_{t}^{t+1} dt' R\left(c(t')\right) \equiv B\left(c(t)\right). \tag{3.2.8}$$

Using $f = B$ in (3.2) or (3.3) yields the Brusselator CML. In the actual simulations, the function B was computed at the start of the calculation by constructing a grid in the phase space of (u, v) values and storing the values of $B(u, v)$ in integer form. Thus, a large numerical mapping specifies the local updating rule.

In order to show how such CMLs may be used to study the spatio-temporal dynamics of oscillatory media, we describe the results of studies of spatial phase resetting and pattern formation in CMLs designed to reproduce the gross features of the Brusselator and complex Ginzburg–Landau reaction–diffusion equations. The problems we address center around the nature of the response of an oscillatory medium to perturbations randomly distributed in space. In particular, we consider the following questions: in the regimes where the system is known to be stable to infinitesimal perturbations, can finite amplitude perturbations excite the system to new persistent spatio-temporal states? How can one design perturbations to elicit particular kinds of responses?

The above problems may be posed more precisely by specifying the class of initial states under consideration. Suppose all nodes of the CML are cycling through their states in synchrony. We than apply a perturbation at phase θ of the oscillation such that a random fraction p of the maps is shifted away from the limit cycle state. More specifically, let $\xi(i)$ be a sequence of independent Boolean random variables with probabilities such that $P(\xi = 1) = p$ and $P(\xi = 0) = 1 - p$. Then, if c_θ is a point on the limit cycle corresponding to phase θ (relative to some arbitrary marker phase), the initial condition is defined as

$$c(i, 0) = c_\Delta \xi(i) + c_\theta (1 - \xi(i)), \tag{3.2.9}$$

where c_Δ represents a shift off the limit cycle characterized by the magnitude Δ. Thus, the initial states may be characterized by three parameters: the initial phase θ, the local

perturbation amplitude Δ, and the average fraction of the lattice that is perturbed p. Of course, average values are computed by averaging over many realizations of the initial perturbation process.

A useful way to attempt to understand the response of such spatially distributed systems lies in an examination of the phase transition curves (PTC). Consider a spatially homogeneous system with a globally attracting limit cycle. This is the usual context in which the PTC is studied [46,91]. Suppose a perturbation with amplitude Δ is applied to the oscillatory system at a phase θ of its oscillation. The PTC is the plot of the asymptotic new phase θ' versus the phase θ. It is clearly a function of the perturbation amplitude Δ. If Δ is small, then θ' will vary through 2π as θ varies through 2π; in this circumstance, the PTC is called type 1 since its average slope is unity. If Δ is large, then it is possible that θ' will only vary over a subinterval of phases as θ varies through one cycle. In this case, the PTC is type 0 since its average slope is zero. If such a transition from type 1 to type 0 behavior occurs as Δ changes, there must be an amplitude Δ and initial phase θ where the PTC is undefined. The system will not relax back to the limit cycle in this case. This is simply a consequence of topological arguments (nonretraction theorem) and has been discussed in detail elsewhere [92].

An analogous problem can be formulated for the spatially distributed oscillatory medium [93]. Suppose it is known that the spatially homogeneous state is stable to small inhomogeneous perturbations. Then, if the system is gently perturbed it will relax back to the spatially homogeneous limit cycle state but with a phase shift. Once again, one may construct a PTC by plotting the asymptotic new phase versus the initial phase at which the stimulus was applied. Of course, the determination of the new phase is much more complicated for the spatially distributed system and was carried out in the following way [93]: following the perturbation, the state of each node on the lattice was monitored at intervals corresponding to the period of the limit cycle. The asymptotic average new phase $\langle \theta' \rangle$ was then determined from a double average over nodes of the lattice and over realizations of the perturbation seeding process.

If the local perturbation strength Δ is sufficiently strong to give rise to type 0 phase resetting, then one might expect interesting behavior as the seeding probability p is varied. For $p = 0$, clearly we have a trivial type 1 response for the system: the new phase is just the initial phase. Type 1 behavior is expected to persist for small p. If $p = 1$, then clearly the system is again equivalent to a homogeneous system and by construction will exhibit type 0 phase resetting since Δ has been chosen to elicit this response. In between, the spatially distributed system must undergo a transition from type 1 to type 0 phase resetting and in analogy to the homogeneous case, one might expect a "singular" response for some values or range of values of p and θ. This is indeed the case for both the complex Ginzburg–Landau and Brusselator models [88,90,93].

In the simulations of both models, the local perturbation consisted of a shift of the phase point off the limit cycle along the u coordinate: $c_\Delta = (u + \Delta, v)$. Figure 12 shows PTCs for the Brusselator model. Phase transition curves with a similar structure have been obtained for the complex Ginzburg–Landau model [88]. In both cases, one sees a transition from type 1 to type 0 behavior as a function of p, and a range of values
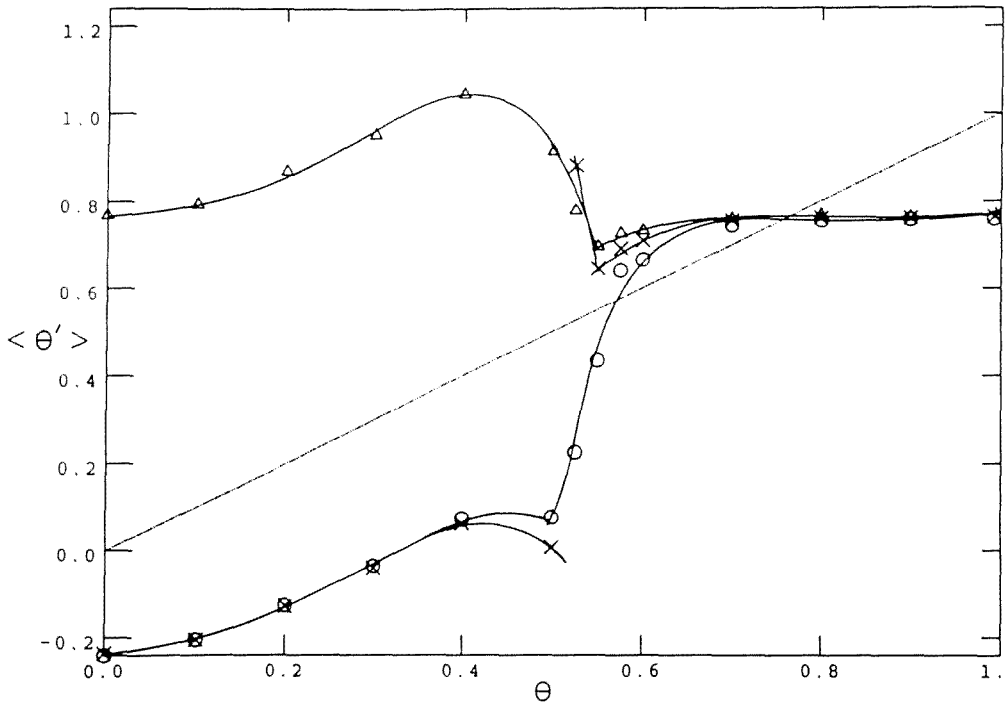
Fig. 12. PTCs for the Brusselator reaction–diffusion CML model showing the transition from type 1 to type 0 behavior as the seeding probability is varied for fixed Δ. The system parameters are $A = 1.0$, $B = 3.5$, $\gamma = 1/16$, $\Delta = 1.0$. The circles are for $p = 0.4$, the crosses for $p = 0.45$, and the triangles for $p = 0.5$.

where the PTC is undefined. For these parameter values, the systems do not relax back to the homogeneous limit cycle but instead form persistent spatio-temporal patterns. The natures of the patterns are, however, different in the two models for the parameter ranges studied. In the complex Ginzburg–Landau model where the oscillations are harmonic in character, one finds chemical turbulence [5,87–89] (cf. fig. 13). The nature of the chemical turbulence in this model has been the subject of a number of studies [5,87–89] for both $\beta \neq 0$ and $\beta = 0$, as is the case for the work described above. Simulations, especially using CMLs, are sufficiently easy that many details of statistical properties like the average number of defects and their correlations have been computed. Also, the regime where the complex Ginzburg–Landau model may be reduced to a nonlinear equation for the local phase has been studied. Such local phase reductions were first carried out by Ortoleva and Ross [94] and later by Kuramoto [5] and Shivasin-sky [95]. The chemical defect-mediated turbulence in the complex Ginzburg–Landau model can serve as a paradigm for a class of turbulent states in a wide range of physical systems and is a topic under active investigation. For further references, see [96]. In the Brusselator where the oscillations are of the relaxation type for a certain range of
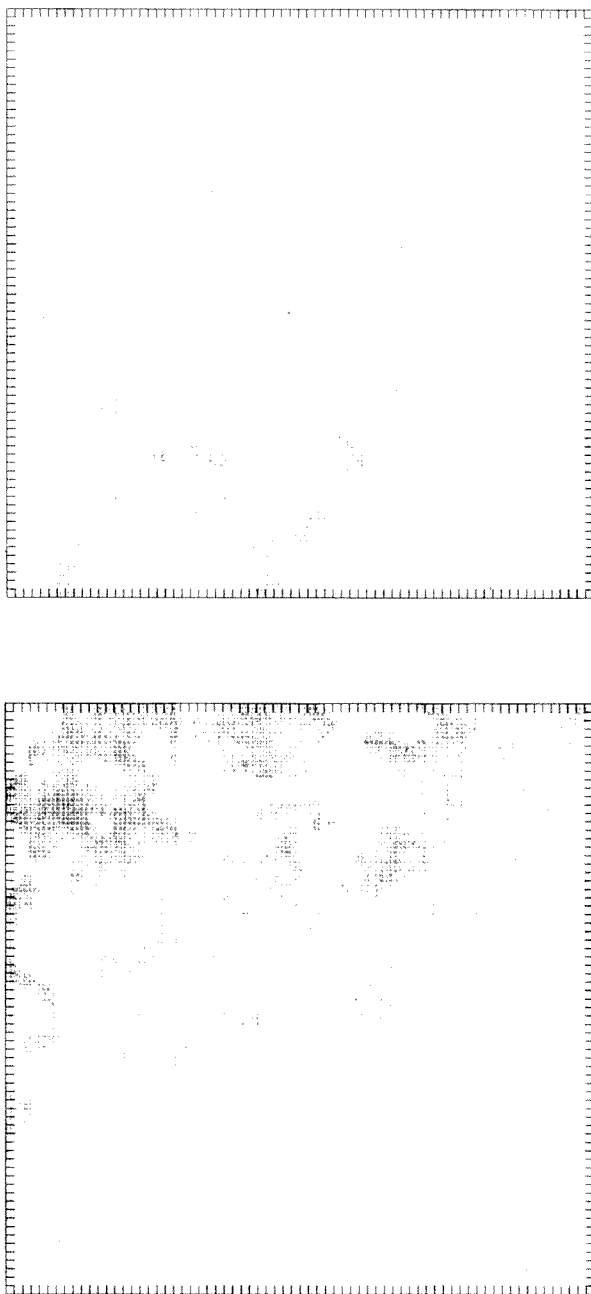
Fig. 13. Chemical turbulence in the complex Ginzburg–Landau model. The left (right) panel shows the phase (amplitude) inhomogeneities in the two-dimensional system after 100 cycles.
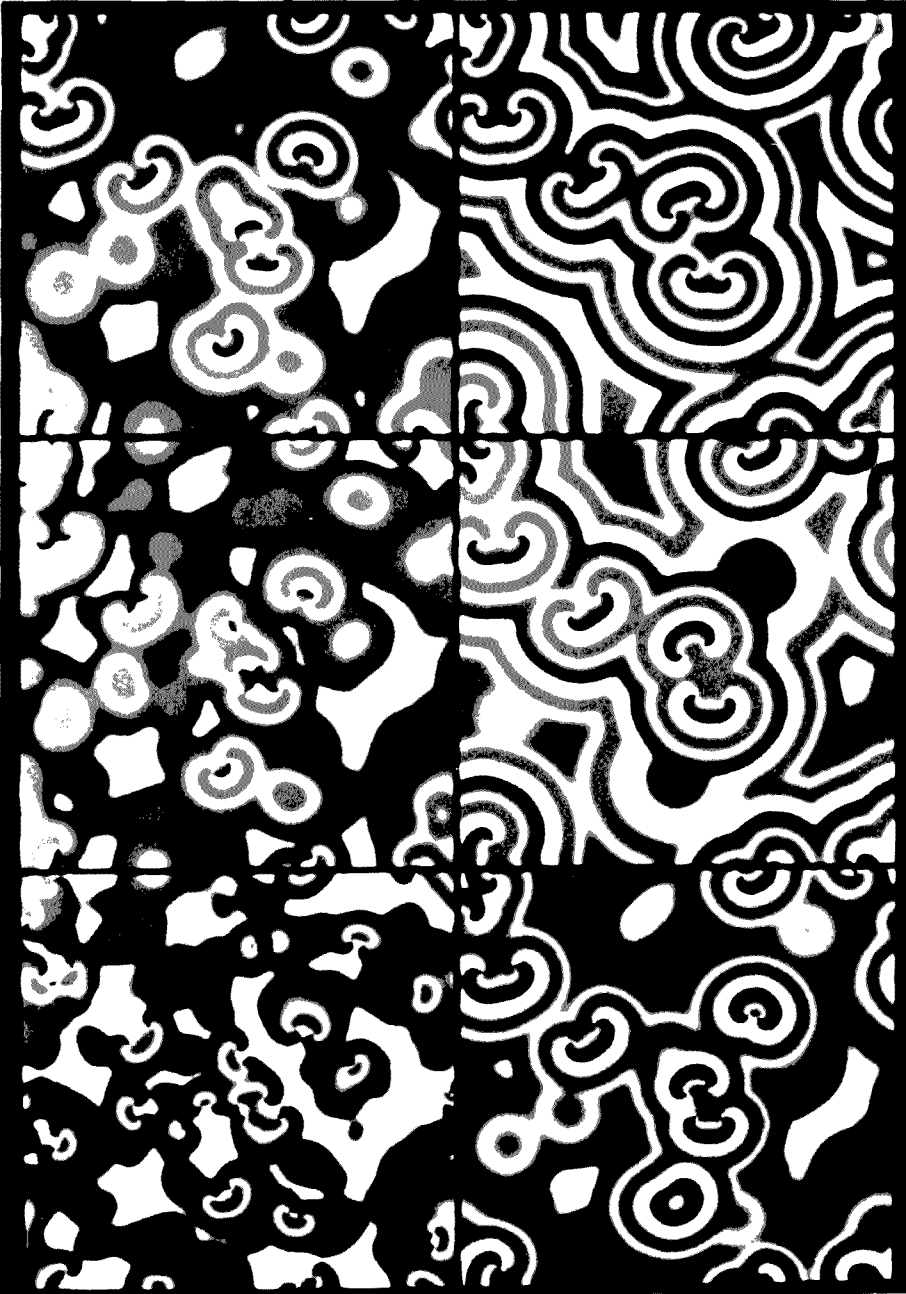
Fig. 14. The inhomogeneous state of the Brusselator CML showing spiral wave formation. System parameters are: $A = 1.0$, $B = 3.5$, $\gamma = 1/16$, $\Delta = 1.0$, $p = 0.45$ and $\phi = 0.52$. The lattice size is 200×200. Configurations are shown for six values of the time, $t = 5, 10, 15, 20, 40, 80$ cycles, increasing from left to right and top to bottom, respectively.

parameters, one finds a random collection of target patterns and, more typically, pairs of counter rotating spiral waves [90]. Examples of such patterns are shown in fig. 14. As the Brusselator parameters are tuned so that the system lies closer to the Hopf bifurcation point, the relaxation oscillations become harmonic in character. However, even before such a change in character occurs, the persistent random distribution of spiral wave pairs like that shown in fig. 12 breaks up and is no longer stable [97]. The nature of the break-up of the spiral wave state and the development of the chemical turbulent state are interesting topics. Both of the CMLs described above are able to reproduce the most robust features of the corresponding reaction–diffusion equations. However, it is possible to construct an even simpler CML that exhibits many of the qualitative features of the phase resetting dynamics and pattern formation processes described and yet is amenable to detailed theoretical analysis [98]. The stability of the homogeneous oscillatory state for *noisy* discrete systems like CMLs and CA has been studied by Bennett et al. [99]. These considerations are important for the investigation of the true asymptotic dynamics in real (noisy) systems.

The utility of the CMLs for the study of these problems lies in the fact that the phenomena are clearly statistical in character due to the random nature of the initial seeding process. Many realizations of the pattern formation process must be carried out in order to properly characterize the response. The above studies allow one to understand how to characterize the perturbations that give rise to very different types of response.

With rather different goals in mind, Babloyantz et al. [100] have carried out a series of studies of both the complex Ginzburg–Landau and Brusselator models, as well as other models, using an Euler-like discretization of the reaction–diffusion equations. Their simulations of these networks of coupled oscillators show interesting properties of the chemical wave dynamics in the presence of obstacles, and applications to robotics are suggested. Discrete models of oscillatory media analogous to the CML models described above have been studied by Hanusse et al. [101].

While the above discussion has concentrated on oscillatory media, we note that these ideas can of course be extended to treat excitable media as well. Such a study has been carried out by Barkley [102] and provides an alternative way to study the problems discussed in some detail in section 2.

Finally, we note that for a class of periodically forced reaction–diffusion equations it is possible to construct directly the CML [103]. However, these systems are rather exceptional, so we have confined our attention to ordinary reaction–diffusion equations.

3.3. PIECEWISE LINEAR MODELS

As an addendum to this section, we briefly describe a class of models for spatial pattern formation processes that have been used for a long time. These models attempt to mimic the behavior of the reaction–diffusion equation (1.1) by replacing the nonlinear chemical kinetics term by a piecewise linear function of the concentration variables. Such a reaction model may be incorporated in a discrete space and time setting to yield a discrete model for the dynamics. The considerations leading to the abstraction of the

chemical kinetics term by a piecewise linear function are analogous to those used to construct the CA rules. The hope is that some deeper analysis of the bifurcation structure may be possible and that the results may be generalized. To some extent this is true, but is difficult because of the discontinuities in the derivatives of the functions and an extension to general cases is not trivial, which limits the utility of this approach. We briefly describe two examples of this type of method.

It is not difficult to construct a simple model that reproduces the general features of the excitable medium automaton [40]. The local excitable dynamics can be modeled by the piecewise linear function $F_e(c)$ of the notional concentration variable c. For a model with l refractory states R_k with numerical values of $-A_k$, we may write $F_e(c)$ as

$$
F_e(c) = \begin{cases}
E_2 = -A & c_1 \le c < c_m , \\
E_1 = 1 & c_2 \le c < c_1 , \\
Q = 0 & -c_3 \le c < c_2 , \\
R_l = -A_l & -c_m < c \le c_{l+2} , \\
R_{l-1} = -A_{l-1} & c_{l+2} \le c < c_{l+1} , \\
\quad \vdots & \\
R_1 = -A_1 & c_4 \le c < c_3 ,
\end{cases}
\tag{3.3.1}
$$

with $c_n > 0$ and c restricted to the interval $(-c_m, c_m)$. If $c_1 < 1$ and $0 < A_1 < A_2 < \ldots < A_l$, the system will exhibit excitability with c_2 as the threshold value. Once the system is in E_1, it will pass to E_2 and then cycle through the series of refractory states R_k ($k = l, l-1, \ldots, 1$) before reaching the resting state $Q = 0$. Of course, this local dynamics is highly schematic, as is reflected in the fact that the "concentration" variable can take on negative values. The excitable medium dynamics can be described by representing the diffusive coupling among local elements by a discrete Laplacian defined on some lattice. Thus, the dynamical evolution of c at site i at time t, $c(i, t)$, is given by

$$
c(i, t+1) = F_e\big(c(i, t)\big) + \frac{d}{2q_n} \sum_{j \in \mathcal{N}} \big(c(j, t) - c(i, t)\big),
\tag{3.3.2}
$$

where d measures the diffusion coupling strength and q_n is the number of neighbors of site i.

Greenberg and Hastings [40] have examined the five-state model in 2-d in detail. In particular, choosing $c_m = 1/(1 - d)$, we have $|c(i, t)| \le c_m$ for all i and t if $|c(i, 0)| \le c_m$. Furthermore, if $c_2/(1 + c_2) < d < u/(1 + u)$, where

$$
u = \min\left(\frac{c_5 - c_4}{2} , \frac{c_4 - c_3}{2} , \frac{c_3}{2} , 1 - c_1 , c_1 \right),
$$

then if $c(i, t)$ is in any region except $[-c_3, c_2)$ its dynamics is independent of the diffusion term. Finally, if

$$0 < \frac{8c_2}{c_1 - c_2 - c_5} \leq d < \frac{c_3}{1 + c_3}, \frac{d^2}{1 - d},$$

then if $-c_3 \leq c(i, t) < c_2$ and at least one of its four neighbors is in $[c_1, c_m)$, then $c_2 \leq c(i, t+1) < c_1$, but if no neighbors are in $[c_1, c_m)$, then $c(i, t+1)$ remains in $[-c_3, c_2)$. These conditions are just those described earlier for the excitable medium automaton; hence, this five-state piecewise continuous model will just reproduce the behavior of the automaton if the parameters are chosen appropriately. However, this model produces dynamics which is a sensitive function of the parameters, and changes in pattern dynamics that are observed do not necessarily correspond to those observed for analogous parameter changes in the underlying reaction–diffusion equation. Therefore, this model has not been exploited to a great degree for exploring the dynamics of such systems. Other piecewise-linear models have also been used to model excitable kinetics and to investigate various aspects of chemical wave propagation processes [104, 105].

The above example dealt with systems with excitable kinetics where the system possesses a stable resting state. Oscillatory systems can show an even richer structure of spatio-temporal states, as was seen in section 3.2. Here, we briefly mention a piecewise continuous model for such systems that was studied by Oono, Kohmoto and Yeung [106]. The essential feature is that the piecewise function $F_e(c)$ for excitable dynamics must be replaced by a function F_o that gives rise to oscillatory kinetics. One such simple function of this type is [106]

$$F_o(c) = \begin{cases} 1 & \text{if } 3/2 \leq c, \\ 0 & \text{if } 1/2 \leq c < 3/2, \\ M & \text{if } c < 1/2. \end{cases} \tag{3.3.3}$$

If $M \in Z$, $M > 1$, the system will cycle through three states. The oscillatory medium model has a somewhat different structure from that described above for the excitable medium. First, the "concentration" at site i at time t is diffusively coupled to that of its neighbors. To this end, a function w is defined as

$$w(i, t) = c(i, t) + \frac{\alpha}{2} \sum_{j \in \mathcal{N}} \left(c(j, t) - c(i, t) \right). \tag{3.3.4}$$

The evolution of the concentration at site i is then given by the updating rule

$$c(i, t+1) = F_o \left(w(i, t) \right). \tag{3.3.5}$$

The 1-d version of this system shows a number of different types of spatio-temporal patterns. Depending on the two control parameters M and α, one observes either two

different types of period-3 states, a turbulent phase, or a soliton-like phase. Some of this structure has been correlated with that observed in the Belousov–Zhabotinsky reaction, but this model must be regarded as a very schematic representation of the full range of behavior of the real chemical system. However, the extensive analytical characterization of the model dynamics and properties carried out in ref. [106] provides an example of the utility of these simple discrete models.

4.   Lattice gas models

Lattice gas cellular automata were introduced a number of years ago [107] as a model that could be potentially useful for the study of fluid flow turbulence that avoided the necessity to solve the Navier–Stokes equation. Roughly, a discrete time dynamics on a lattice was constructed, where particles move with discrete velocities from node to node. Typically, in order to simplify the dynamics, an exclusion principle is assumed whereby no two particles at a given node may have the same velocity. Collisions may occur at the nodes which give rise to changes in the particles' velocities. Provided the collision rules are such that the microscopic dynamics satisfies mass and momentum conservation then, under suitable conditions, the macroscopic velocity field can be shown to satisfy a Navier–Stokes equation. So the idea is that if one is interested primarily in the dynamics of macroscopic fields then, provided the microscopic dynamics satisfies a few basic conditions, its precise nature is unimportant. The implementation of the above scheme involves the study of a number of subtle questions, which are discussed in detail elsewhere [107–111], but it has been successful in producing turbulent flow patterns like that of real fluids. The purpose of this section is to describe how these ideas can be carried over into the domain of chemically reacting systems.

For a chemically reacting system, one must construct a contrived reactive molecular dynamics that preserves the essential features of the real reacting microscopic dynamics. In particular, the correct conservation laws and chemical reaction mechanisms must be incorporated in the microscopic dynamics if the macroscopic concentration field is to satisfy a reaction–diffusion equation. By going to this level of description, we gain the feature that the effects of internal fluctuations on the evolution of the macroscopic concentration fields can in principle be studied. At the very least, one has the opportunity to design fluctuations at the "molecular" level rather than simply appending random force terms to the reaction diffusion or CML models. Below we describe several different lattice gas models that have been used to study reactive systems.

4.1.   REACTIVE LATTICE GAS AUTOMATON

A lattice gas model that corresponds on the macroscopic level to an arbitrary polynomial chemical rate law has been constructed [112–114] and will be outlined here. The case of a single intermediate chemical species X will be described, but the extension to several species can be carried out. The general formulation of the single intermediate species case is described at length in ref. [114]. In order to present the idea behind the

model in a simpler form, we restrict consideration to a specific reaction scheme, the Schlögl model that has already been described in section 3.1. This also has the advantage that we can contrast the lattice gas description with that of the CML for the same problem. The reaction mechanism and chemical rate law for the Schlögl model are given in (3.1.1) and (3.1.2), respectively. The goal is to construct a discrete microscopic dynamics that is consistent with these kinetics. In qualitative terms, the model is constructed in the following way: space and time are discrete and the particles are assumed to move with discrete velocities on the lattice. The reaction medium in general consists of solvent molecules as well as reactive species. In the nonequilibrium domain, the concentrations of certain chemical species are assumed to be held fixed in order to maintain the system out of equilibrium. For the Schlögl model, this is the case for the A, B and C species. Hence, the time dependence of only one chemical concentration X is of interest. In the reactive lattice gas automaton, the dynamics of the solvent molecules and the constrained species is not explicitly considered. The nodes of the lattice are assumed to be occupied by "ghost" particles whose effect on the X species is to produce elastic collisions as well as reactive collisions, in accord with the reaction scheme. Since the dynamics of these other species is not explicitly considered, their effects are embodied in a set of rules specifying the stochastic dynamics of the X particles at a node. The elastic collisions are modeled by random rotations of the particle configuration, while the reactive collisions are modeled by a combination of probabilistic rules for the increase or decrease of the number of X particles, together with a random rotation to mimic the velocity change that will accompany the reactive collision. A mathematical description of this set of operations is easily written.

The X particles are assumed to move on a square lattice $\mathcal{L}$ with periodic boundary conditions. At each node of the lattice labeled by a discrete vector r there are four cells labeled by an index i that is associated with unit velocity vectors c_i along the lattice directions. The exclusion principle mentioned above is assumed to apply so that each cell (r, i) can be coded by a Boolean variable $s_i(r)$,

$$s_i(r) = \begin{cases} 1 & \text{cell occupied,} \\ 0 & \text{cell unoccupied.} \end{cases} \tag{4.1.1}$$

A configuration of particles at a node at time k may then be described by a random vector $\eta(k, r)$ that takes on values in the space of all 16 four-bit words. Thus, a configuration of the whole lattice at time k is described by the Boolean field

$$\eta(k) = \{\eta(k, r) : r \in \mathcal{L}\}, \tag{4.1.2}$$

that takes on values in a phase space of all possible assignments

$$s(\cdot) = \{s(r) = \langle s_i(r)\rangle_{i=1}^4 : r \in \mathcal{L}\}. \tag{4.1.3}$$

The evolution of the system is now embodied in a set of rules that specify how the Boolean random fields evolve in time. For the chemically reacting system under consideration, one time step in the evolution is accomplished by the product of three transformations: a propagation step P where particles move from node to node, as well as the chemical transformation C and rotation R operations described above; their explicit forms will be given below. Microdynamical equations that play the role of the equations of motion for a classical many-body system can now be written for the random fields $\eta_i(k, r)$.

The propagation and rotation transformations are easily written. Since each particle moves one lattice unit in the direction of its velocity, for the configuration after propagation $\eta_i^P(k, r)$, we have

$$P : \eta_i^P(k, r) = \eta_i(k - 1, r - c_i). \tag{4.1.4}$$

The rotation operator R consists of random rotations by $\pm \pi/2$ of the configuration, so

$$R : \eta_i^R(k, r) = \xi_{\pi/2} \eta_{i+3} + (1 - \xi_{\pi/2}) \eta_{i+1}, \tag{4.1.5}$$

where η^R denotes the configuration after rotation and $\xi_{\pi/2}$ is a Boolean random variable with probability $P(\xi_{\pi/2} = 0) = P(\xi_{\pi/2} = 1) = 1/2$. In (4.1.5), the subscript addition is modulo four.

The chemical transformation step C is a little more complicated. At each node of the lattice, independent of the others, particles are created or destroyed, giving rise to local reactions of the form $\alpha X \to \beta X$ with reaction probabilities $P_{\alpha\beta}$ independent of their velocity state. Of course, if no reaction occurs we have $\alpha = \beta$ and

$$P_{\alpha\alpha} = 1 - \sum_{\alpha \neq \beta} P_{\alpha\beta}. \tag{4.1.6}$$

There are two elements that are needed to write a formal expression of C: we must specify the initial configuration with, say, α particles, and we must ensure that the chemical transformation $\alpha \to \beta$ occurs with the appropriate probability. Consider a specific example where the node contains no particles of species X. The following product of Boolean random variables will ensure that this is the case:

$$Q^0(\eta) = \prod_{i=1}^{4} (1 - \eta_i). \tag{4.1.7}$$

Clearly, if there are no particles initially at a node, then the particle number can either remain the same or increase from one to four. If we consider the reaction $C \to X + B$ in the Schlögl mechanism (3.1.1), this corresponds to $0 \to X$ in the present terminology and occurs with probability P_{01}. To code this, we introduce random variables $\xi_i^{\alpha\beta}$ with distributions determined in the following way: we define the product

$$\gamma_i^{01} = \xi_i^{01} \prod_{j \neq 1}^{4} \left(1 - \xi_j^{01}\right) \prod_{\tau \in R(01)} \prod_{m=1}^{4} \left(1 - \xi_m^{0\tau}\right), \qquad (4.1.8)$$

where $R(\alpha)$ is the set of all allowed reactions for each a. Then, if $\beta \in R(\alpha)$ we define $R(\alpha\beta) = R(\alpha) - \{\beta\}$. The first factor of ξ_i^{01} ensures that if the reaction produces a particle at i, then another will not be created in the other velocity directions, while the second factor ensures that the other reactions that are possible from an initial state with α particles do not take place. The probability distribution for γ^{01} is

$$Pr\left(\gamma^{01} = 1\right) = P_{01}/4, \quad Pr\left(\gamma^{01} = 0\right) = 1 - P_{01}/4, \qquad (4.1.9)$$

where the factor 4 comes from the fact that there are four distinct outcomes of the reaction since the particle can be created in any of the four velocity states. The overall contribution of this reaction type to the value of η_i after the chemical transformation step η_i^C is

$$Q^0(\eta)\gamma^{01}. \qquad (4.1.10)$$

The full expression for η_i^C follows from a sum over all possible reaction types and is given in ref. [114].

The microdynamical equations of motion for the automaton are now easily written as

$$\eta_i(k,r) = \xi_{\pi/2}\, \eta_{i+3}^C(k-1, r-c_i) + (1 - \xi_{\pi/2})\, \eta_{i+1}^C(k-1, r-c_i). \qquad (4.1.11)$$

This equation can serve as the basis of a discussion of the dynamics of the automaton and the consideration of various kinetic and macroscopic equation limits of the full dynamics. In particular, if one assumes that one may factor averages of products of the random variables and considers a spatially homogeneous system in equilibrium in velocity space, (4.1.11) reduces to the chemical rate law

$$\frac{d\rho(t)}{dt} = \kappa_0 - \kappa_1\, \rho(t) + \tfrac{3}{8}\, \kappa_2\, \rho^2(t) - \tfrac{1}{16}\, \kappa_3\, \rho^3(t) + \tfrac{1}{256}\, \kappa_4\, \rho^4(t). \qquad (4.1.12)$$

An interesting feature of this construction (and the passage from microscopic to macroscopic descriptions in general) is that there are many (an infinite number of) microscopic CA models that give rise to the same macroscopic law. There are twenty independent elementary reaction probabilities $P_{\alpha\beta}$ but only five independent macroscopic rate coefficients κ_n. Thus, the same rate law may be obtained from different microscopic models even when one eliminates elementary reactions that do not appear in a particular mechanism. For example, in the Schlögl model there are only eight elementary reactions (reverse reactions included), but this is still larger than the number of rate coefficients. In general, each microscopic CA model will give rise to different internal fluctuations and hence possibly different macroscopic behavior.
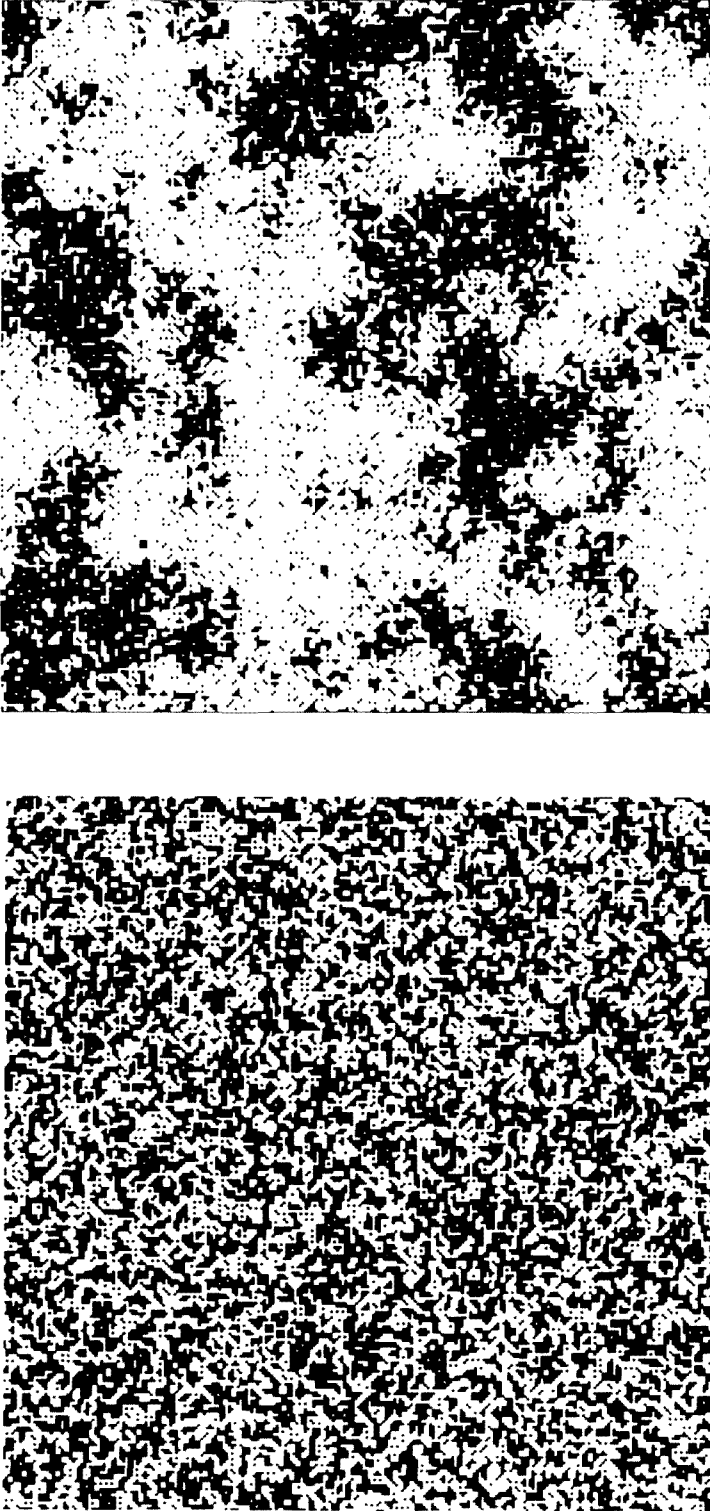
Fig. 15. Evolution from the unstable state for the Schlögl LGCA model. The left panel is for $t = 2$, while the right panel is for $t = 300$. The system parameters are $\kappa_0 = 0.002$, $\kappa_1 = 0.039$, $\kappa_2 = 0.19$ and $\kappa_3 = 0.49$.

Simulations have been carried out on one version of the Schlögl model. The results show that the CA model is able to reproduce the phase separation dynamics that is expected if the system is in the (deterministic) bistable region and is initially prepared in the unstable state. The results of such simulations are shown in fig. 15 and may be compared with those of fig. 9 for the CML for this system. Clearly, the qualitative structure of the domain formation is the same in the late stages of the growth. Detailed properties of the domain growth for the LGCA remain to be investigated.

4.2. TURBULENT REACTIVE FLOWS

The study of turbulent reactive flows requires the inclusion of the dynamics of the fluid velocity field in the macroscopic description. As is well known [107], the choice of lattice is crucial for LGCA models of the Navier–Stokes equations in order that isotropy of the stress tensor may be maintained. Simulations in two space dimensions must be carried out on a triangular lattice and 3-d simulations on a 4-d hypercubic lattice in order to preserve such isotropy to second order in the Mach number. For reactive turbulent flows, one must deal simultaneously with the complexities that arise from chemical reactions as well as those related to the correct description of the fluid flow field.

Since in the general case the investigation of chemically reacting flows entails the study of multi-component fluids, additional difficulties concerning the Galilean invariance of the macroscopic equations derived from the LGCA arise. The macroscopic equations derived from the LGCA take the form [115]

$$\frac{\partial \rho}{\partial t} + \nabla \cdot (\rho u) = 0, \tag{4.2.1a}$$

$$\frac{\partial \rho u}{\partial t} + \nabla \cdot (g \rho u u) = -\nabla p + \nu \nabla^2 (\rho u) + \nu_b \nabla (\nabla \cdot (\rho u)), \tag{4.2.1b}$$

$$\frac{\partial \rho_\alpha}{\partial t} + \nabla \cdot (\rho_\alpha u) = D \nabla^2 \rho_\alpha, \tag{4.2.1c}$$

where ρ_α is the average concentration per site of species α, ρ is the total density, u is the average velocity field, ν is the kinematic shear viscosity, ν_b is the kinematic bulk viscosity, and p is the pressure field. Due to the presence of the density-dependent factor g, these equations are not Galilean invariant. For a one-component incompressible fluid the Navier–Stokes equations are recovered if time, pressure and viscosity are scaled. However, since g is not present in the equation for the species densities, such scaling cannot reduce the multi-component equations to the normal hydrodynamic form.

In spite of these difficulties, there have appeared LGCA models for special examples of turbulent reactive flows. Calvin et al. and Zehnle and Searby [116] have simulated a simple reaction $A + B \rightarrow 2C$ in a turbulent fluid flow. In their model, two binary bits

are used for each of the six velocity directions on the triangular lattice. These four two-bit words are used to code the four possible states of a lattice gas cell: $\{0, A, B, C\}$, where 0 is the empty cell and A, B and C label cells occupied by the respective chemical species. Thus, there are twelve binary bits to code the moving particles. In addition, the model allows for the presence of from zero to three fixed particles per site, and four additional bits are used to code for the presence of these rest particles. The existence of rest particles is crucial since with suitable dynamics (see ref. [116] for full details of the CA rule), one can construct a model with pseudo Galilean invariance where $g(\rho)$ is a maximum.

The simulations of this model show interesting structure. In order to study a reactive shear layer that develops a Kelvin–Helmholtz instability, a 2-d box of 1024×512 sites was filled in the upper half with A particles and in the lower half with B particles, with equal and opposite velocities. The irreversible reaction $A + B \rightarrow 2C$ occurs at the interface. For the given conditions, the reaction does not couple to the fluid flow field, but the development of an instability at the interface has a marked effect on the reaction rate, which deviates substantially from the predictions of a simple diffusion controlled reaction rate model [116].

LGCA models show considerable promise for the study of a variety of problems involving chemical reactions in fluids. For instance, they can be used to explore the chemical wave propagation processes described in sections 2 and 3. Since fluctuations are incorporated, these models can complement Langevin equation and other stochastic model studies of bifurcations and chemical wave dynamics [117, 118]. The development of LGCA is still at a very early stage and the above description simply provides a few examples and possible formulations of such models.

5.   Conclusions

The validity of the discrete models described here relies on the assumption (verified in some instances) that one can do quite a bit of violence to the dynamics of the system and yet obtain reasonable results. Stated in other terms, if the basic elements of a mechanism or microscopic process are understood and incorporated in the construction of discrete models, the gross aspects of the spatio-temporal structure should also follow from the model dynamics. Thus, discrete models are attractive from two points of view. First, for the trivial but important reason that they are usually orders of magnitude more computationally efficient than direct solutions of the reaction–diffusion equations. Second, when one has successfully built such a model, one can be reasonably certain that the essence of a mechanism for the evolution is understood. Hence, one has accomplished one of the usual goals of science, namely, the abstraction of a complex physical process in a simple model.

It is worth mentioning that a number of related models have been intentionally omitted from this review. There is a body of literature dealing with birth–death master equation descriptions of the dynamics of spatially distributed systems [86, 119]. Such models have been used to explore fluctuation effects on the bifurcation structure in reaction–diffusion systems. There has recently been a considerable amount of research

on discrete reaction–diffusion models, such as interacting particle systems [120] and reactive random walk models on regular and fractal lattices, which have been used to explore the validity of macroscopic rate laws [121]. Depending on the dimension and reaction mechanism, a phenomenological description of the rate process may no longer apply. The LGCA models described in section 4 can also be used to examine these questions at a level of description that includes particle velocities as well as numbers.

Discrete models provide a simple way to describe complex processes. It is interesting to see how complex dynamics can follow from a simple and apparently trivial rule. It is equally interesting to see that a seemingly complex spatio-temporal structure may have a simple physical and mathematical basis. It seems clear that such models will occupy a prominent place in the study of complex chemical systems.

Acknowledgements

References

[1]   See, for example, R.J. Field and M. Burger (eds.), *Oscillations and Traveling Waves in Chemical Systems,* (Wiley, New York, 1986);
      P. Bergé, Y. Pomeau and C. Vidal, *Order Within Chaos* (Wiley, New York, 1984);
      G. Nicolis and F. Baras (eds.), *Chemical Instabilities* (Reidel, Dordrecht, 1984).
[2]   See, for example, P. Fife, in: *Non-Equilibrium Dynamics in Chemical Systems,* ed. C. Vidal and A. Pacault (Springer, Berlin, 1984), p. 76.
[3]   B. Halperin and P. Hohenberg, Rev. Mod. Phys. 49(1977)435.
[4]   A.C. Newell, in: *Lectures in Applied Mathematics,* Vol. 15 (Amer. Math. Soc., Providence, 1974).
[5]   Y. Kuramoto, *Chemical Oscillations, Waves and Turbulence* (Springer, Berlin, 1980).
[6]   J. Von Neumann, *Theory of Self-Reproducing Automata,* ed. A.W. Burks (University of Illinois, Urbana, 1966).
[7]   E.F. Codd, *Cellular Automata* (Academic Press, New York, 1986);
      G. Langton, Physica D10(1984)135.
[8]   S. Wolfram, Rev. Mod. Phys. 55(1983)601.
[9]   D. Farmer, T. Toffoli and S. Wolfram (eds.), *Cellular Automata* (North-Holland, Amsterdam, 1984);
      S. Wolfram (ed.), *Theory and Applications of Cellular Automata* (World Scientific, Singapore, 1986);
      J. Demongeot, E. Cole and M. Tchuente, *Dynamical Systems and Cellular Automata* (Academic Press, New York, 1985).

[10] J.T. Tyson and J.P. Keener, Physica D33(1988)327.

[11] A.T. Winfree, SIAM Rev. 32(1990)1.

[12] J. Grasman, *Asymptotic Methods for Relaxation Oscillations and Applications* (Springer, New York, 1987).

[13] N. Wiener and A. Rosenblueth, Arch. Inst. Cardiol. Mexico 16(1946)205.

[14] A.T. Winfree, Science 175(1972)634; ibid. 181(1973)937.

[15] G.K. Moe, W.C. Rheinboldt and J.A. Abildskov, Amer. Heart J. 67(1964)200;
     G.K. Moe and J.A. Abildskov, Amer. Heart J. 58(1959)59.

[16] V.I. Krinsky, Biophys. 11(1966)676.

[17] D.T. Kaplan, J.M. Smith, B.E.H. Saxberg and R.J. Cohen, Math. Biosci. 90(1988)19.

[18] L.V. Reshodko and J. Bures, Biol. Cybernetics 18(1975)181.

[19] P. Foerster, S.C. Müller and B. Hess, Science 241(1988)685.

[20] J.P. Keener, SIAM J. Appl. Math. 46(1986)1039;
     J.P. Keener and J.J. Tyson, Physica D21(1986)307.

[21] E. Meron and P. Pelcé, Phys. Rev. Lett. 60(1988)1880;
     E. Meron, Phys. Rev. Lett. 63(1989)684.

[22] A.V. Holden, M. Markus and H.G. Othmer (eds.), *Nonlinear Wave Processes in Excitable Media* (Plenum Press, New York, 1991).

[23] V.S. Zykov, *Simulation of Wave Processes in Excitable Media* (Manchester University Press, Manchester, 1987).

[24] S.C. Müller, T. Plesser and B. Hess, Science 230(1985)661.

[25] O.E. Rössler and C. Kahlert, Z. Naturforsch. 34a(1979)565.

[26] W. Jahnke, W.E. Skaggs and A.T. Winfree, J. Chem. Phys. 93(1989)740.

[27] G. Skinner and H.L. Swinney, Physica D, to be published.

[28] D. Barkley, M. Kness and S. Tuckerman, Phys. Rev. A42(1990)2489.

[29] C. Elphick and E. Meron, *Spiral Vortex Interactions*, to be published;
     S. Rica and E. Tirapegui, Phys. Rev. Lett. 64(1990)878.

[30] A.T. Winfree and W. Jahnke, J. Phys. Chem. 93(1989)2823;
     A.T. Winfree and S.H. Strogatz, Physica D8(1983)35; ibid. 13(1984)221.
     P.J. Nandapurkar and A.T. Winfree, Physica D29(1987)69;
     J.P. Keener, Physica D31(1988)269.

[31] A.T. Winfree, E.M. Winfree and H. Seifert, Physica D17(1985)109;
     A.V. Panfilov and A.T. Winfree, Physica D17(1985)323.

[32] S.J. Fraser and Y.S. Kan, Nucl. Phys. B 5A(1988)241;
     A.J. Irwin and S.J. Fraser, J. Chem. Phys., to be published.

[33] S. Fraser and R. Kapral, J. Chem. Phys. 85(1986)5682.

[34] D. Stauffer, Phys. Rep. 54(1979)1.

[35] E.N. Gilbert, SIAM J. Appl. Math. 9(1961)533.

[36] R.M. Bradley, J. Chem. Phys. 86(1987)7245.

[37] W.A. Johnson and R. Mehl, Trans. AIME 135(1939)416;
     M. Avrami, J. Chem. Phys. 7(1939)1103: ibid. 8(1940)212.

[38] M. Weinberg and R. Kapral, J. Chem. Phys. 91(1989)7189.

[39] R. Fisch, J. Gravner and D. Griffeath, unpublished.

[40] J.M. Greenberg, B.D. Hassard and S.P. Hastings, Amer. Math. Soc. 84(1978)1296;
     J.M. Greenberg and S.P. Hastings, SIAM J. Appl. Math. 34(1978)515.

[41] D. Griffeath, Notices Amer. Math. Soc. 35(1988)1472.

[42] M. Markus and B. Hess, in: *Dissipative Structures in Transport and Combustion*, Vol. 48, ed. D. Meinköhn (Springer, Heidelberg, 1990), p. 197.
     M. Markus and B. Hess, Nature 347(1990)56.

[43] M. Gerhardt, H. Schuster and J.J. Tyson, Science 247(1990)1563.

[44] W. Freedman and B. Madore, Astrophys. J. 265(1983)140;
W. Freedman and B. Madore, Science 222(1983)615;
L.S. Schulman and P.E. Seiden, Science 233(1986)425.

[45] A.L. Hodgkin and A.F. Huxley, J. Physiol. 117(1952)500;
D. DiFrancesco and D. Noble, Phil. Trans. Roy. Soc. B307(1985)353.

[46] A.T. Winfree, *The Geometry of Biological Time* (Springer, New York, 1980).

[47] A.T. Winfree, *When Time Breaks Down: The Three Dimensional Dynamics of Electrochemical Waves and Cardiac Arrythmias* (Princeton University Press, Princeton, 1987).

[48] B.P. Belousov, in: *Sbornik Referatov po Radiatsionni Meditsine* (Medgiz, Moscow, 1958);
A.M. Zhabotinsky, Biofizika 9(1964)306.

[49] See, for example, R.M. Berne and M.N. Levy, *Cardiovascular Physiology* (C.V. Mosby, St. Louis, 1981);
A.M. Katz, *Physiology of the Heart* (Raven Press, New York, 1977).

[50] J.M. Smith, A.L. Ritzenberg and R.J. Cohen, Comp. Cardiol. 201(1983);
J.M. Smith and R.J. Cohen, Proc. Natl. Acad. Sci. USA 81(1984)233.

[51] M.-N. Chee, S.G. Whittington and R. Kapral, Physica D32(1988)437.

[52] J. Maselko, J.S. Reckley and K. Showalter, J. Phys. Chem. 93(1989)2774.

[53] J. Maselko and K. Showalter, Physica D, to be published.

[54] W.Y. Tam, W. Horsthemke, Z. Noszticius and H.L. Swinney, J. Chem. Phys. 88(1988)3395.

[55] V. Castets, E. Dulos, J. Boissonade and P. DeKepper, Phys. Rev. Lett. 64(1990)2953.

[56] W.Y. Tan, J.A. Vastano, H.L. Swinney and W. Horsthemke, Phys. Rev. Lett. 61(1988)2163;
Q. Quang, J. Boissonade, J.-C. Roux and P. DeKepper, Phys. Lett. A134(1989)282.

[57] A.M. Turing, Phil. Trans. Roy. Soc. B237(1952)37.

[58] A. Arneodo and J. Elezgaray, Phys. Lett. A143(1990)25;
A. Arneodo, J. Elezgaray, J. Pearson and T. Russo, Instabilities in front patterns in reaction–diffusion systems, to be published;
J.A. Vastano, T. Russo and H.L. Swinney, Physica D46(1990)23.

[59] R.J. Shwankner, M. Eiswirth, P. Moller, K. Wetzl and G. Ertl, J. Chem. Phys. 87(1987)742;
P. Moller, K. Wetzl, M. Eiswirth and G. Ertl, J. Chem. Phys. 85(1986)5328.

[60] R.M. Ziff, E. Gulari and Y. Barshad, Phys. Rev. Lett. 56(1986)2553.

[61] M. Gerhardt and H. Schuster, Physica D36(1989)209.

[62] B. Chopard and M. Droz, J. Phys. A21(1988)205.

[63] A. Canning and M. Droz, Physica D, to be published.

[64] H.S. Berryman and R. Franceschetti, Phys. Lett. A136(1989)348.

[65] H. Hartman and P. Tamayo, Physica D, to be published.

[66] I. Waller and R. Kapral, Phys. Rev. A30(1984)2047;
R. Kapral, Phys. Rev. A31(1985)3868.

[67] K. Kaneko, Prog. Theor. Phys. 72(1984)480: ibid. 74(1985)1033.

[68] R.J. Diessler, Phys. Lett. A100(1984)451.

[69] J.P. Crutchfield and K. Kaneko, in: *Directions in Chaos*, ed. Hao Bai-lin (World Scientific, Singapore, 1987);
K. Kaneko, Physica D34(1989)1;
K. Kaneko, in: *Formation, Dynamics and Statics of Patterns*, ed. K. Kawasaki (World Scientific, Singapore, 1989);
R. Kapral, M.-N. Chee, S.G. Whittington and G.-L. Oppo, in: *Measures of Complexity and Chaos*, ed. N.B. Abraham, A.M. Albano, A. Passamante and P.E. Rapp (Plenum, New York, 1989), p. 381;
R. Kapral, in: *Self-Organization, Emerging Properties and Learning*, ed. A. Babloyantz (Plenum, New York, 1990).

[70] See, for example, J. Boissonade and P. DeKepper, in: *Oscillations and Traveling Waves in Chemical Systems,* ed. R.J. Field and M. Burger (Wiley, New York, 1985);
M. Alamgir and I. Epstein, J. Amer. Chem. Soc. 105(1983)2500;
P. Lamba and J.L. Hudson, Chem. Engin. Comm. 32(1985)369;
P. Rehmus, W. Vance and J. Ross, Chem. Phys. 80(1984)373;
I. Epstein, J. Phys. Chem. 88(1984)187.

[71] F. Schlögl, Z. Phys. 253(1972)147;
F. Schlögl, C. Escher and R.S. Berry, Phys. Rev. A27(1983)2698.

[72] A. Hanna, A. Saul and K. Showalter, J. Amer. Chem. Soc. 104(1982)3838;
A. Saul and K. Showalter, in: *Oscillations and Traveling Waves in Chemical Systems,* ed. R.J. Field and M. Burger (Wiley, New York, 1985), p. 419.

[73] J.R. Roebuck, J. Phys. Chem. 6(1902)365;
J.N. Pendlebury and R.H. Smith, Int. J. Chem. Kin. 6(1974)663.

[74] J.D. Gunton, M. San Miguel and P. Sahni, in: *Phase Transitions and Critical Phenomena,* ed. C. Domb and J.L. Lebowitz (Academic Press, New York, 1983).

[75] S.M. Allen and J.W. Cahn, Acta Metall. 27(1979)1085.

[76] R. Kapral and G.-L. Oppo, Physica D23(1986)455;
G.-L. Oppo and R. Kapral, Phys. Rev. A36(1987)5820.

[77] G.-L. Oppo and R. Kapral, in: *Spatial Inhomogeneities and Transient Behavior in Chemical Kinetics,* ed. P. Gray, G. Nicolis, F. Baras, P. Borckmans and S.K. Scott (Manchester University Press, Manchester, 1990), p. 335.

[78] T.M. Rogers, K.R. Elder and R.C. Desai, Phys. Rev. B37(1988)9638;
R. Elder, T.M. Rogers and R.C. Desai, Phys. Rev. B38(1988)4725.

[79] B. Widom and J. Rowlinson, *The Molecular Theory of Capillarity* (Clarendon Press, Oxford, 1982).

[80] A.M. Albano, N.B. Abraham, D.E. Chyba and M. Martelli, Amer. J. Phys. 52(1983)161.

[81] S. Puri, R.C. Desai and R. Kapral, Coupled map model with a conserved order parameter, Physica D, to be published.

[82] V.L. Prokrovsky, J. de Phys. 42(1981)761;
P. Bak and V.L. Prokovsky, Phys. Rev. Lett. 47(1981)958;
S.E. Burkov, V.L. Prokovsky and G. Uimim, J. Phys. A15(1982)L645;
S. Aubry, in: *Bifurcation Phenomena in Mathematical Physics,* ed. C. Bardis and D. Bessis (Reidel, Dordrecht, 1981).

[83] Y. Oono and S. Puri, Phys. Rev. Lett. 58(1987)836.

[84] S. Puri and Y. Oono, Phys. Rev. A38(1988)1542.

[85] I. Prigogine and R. Lefever, J. Chem. Phys. 48(1968)1695.

[86] G. Nicolis and I. Prigogine, *Self Organization in Nonlinear Systems* (Wiley, New York, 1977).

[87] T. Bohr, A.W. Pedersen, M.H. Jensen and D.A. Rand, in: *New Trends in Nonlinear Dynamics and Pattern Forming Processes,* ed. P. Coullet and P. Heurre (Plenum, New York, 1989).

[88] X.-G. Wu and R. Kapral, J. Chem. Phys., to be published.

[89] P. Coullet, L. Gil and J. Lega, Phys. Rev. Lett. 62(1989)161.

[90] M.-N. Chee, R. Kapral and S.G. Whittington, J. Chem. Phys. 92(1990)7315.

[91] E.N. Best, Biophys. J. 27(1979)87;
M.R. Guevara and L. Glass, J. Math. Biol. 14(1982)1;
L. Glass, M.R. Guevara, J. Belair and A. Shrier, Phys. Rev. A29(1984)1348;
L. Glass and A.T. Winfree, Amer. J. Physiol. 246(1984)251.

[92] M. Kawato, J. Math. Biol. 12(1981)13;
M. Kawato and R. Suzuki, Biol. Cyber. 30(1978)241;
S. Strogatz, Math. Intelligenzer 7(1985)9.

[93] M.-N. Chee, R. Kapral and S.G. Whittington, J. Chem. Phys. 92(1990)7302.

[94] P. Ortoleva and J. Ross, J. Chem. Phys. 60(1974)5090.

[95] G.I. Shivasinsky, Acta Astronaut 4(1977)1177.

[96] P. Coullet, in: *Measures of Complexity and Chaos,* ed. N.B. Abraham, A.M. Albano, A. Passamante and P.E. Rapp (Plenum, New York, 1989).

[97] M.-N. Chee, X.-G. Wu and R. Kapral, to be published.

[98] R. Livi and R. Kapral, to be published.

[99] C.H. Bennett, G. Grinstein, Y. He, C. Jayaprakash and D. Mukamel, Phys. Rev. A41(1990)1932.

[100] A. Babloyantz, J.A. Sepulchre and L. Steels, A network of oscillators can perform tasks without prior training, to be published;
A. Babloyantz and J.A. Sepulchre, Front propagation into unstable media: A computational tool, to be published.

[101] P. Hanusse, Perez-Munuzuri and C. Vidal, in: *Nonlinear Wave Processes in Excitable Media,* ed. A.V. Holden, M. Markus and H.G. Othmer (Plenum, New York, 1991).

[102] D. Barkley, in: *Proc. Pushchino Conf. on Waves in Excitable Media,* Physica D, to be published..

[103] J.D. Keeler, An explicit relation between coupled maps, cellular automata and reaction–diffusion equations, UCSD Preprint (1986);
J.D. Keeler and J.D. Farmer, Physica D23(1986)413.

[104] A.T. Winfree, Sci. Amer. 230(1974)82.

[105] J.J. Tyson and P.C. Fife, J. Chem. Phys. 73(1980)2224.

[106] Y. Oono and M. Kohmoto, Phys. Rev. Lett. 35(1985)2927;
see also Y. Oono and C. Yeung, J. Stat. Phys. 48(1987)593.

[107] J. Hardy, O. de Pazzis and Y. Pomeau, Phys. Rev. A13(1976)1949;
U. Frisch, B. Hasslacher and Y. Pomeau, Phys. Rev. Lett. 56(1986)1505.

[108] D. d'Humiéres, B. Hasslacher, P. Lallemand, Y. Pomeau and J.P. Rivet, Complex Systems 1(1987)648.

[109] P. Manneville, N. Boccara, G.Y. Vichniac and R. Bidaux (eds.), *Cellular Automata and Modeling of Complex Physical Systems* (Springer, Berlin, 1989).

[110] D. D'Humiéres, Y.H. Quain and P. Lallemand, in: *Discrete Kinetic Theory, Lattice Gas Dynamics and the Foundations of Hydrodynamics,* ed. I.S.I. and R. Monaco (World Scientific, Singapore, 1989), p. 102.

[111] G. Doolen (ed.), *Lattice Gas Methods for Partial Differential Equations* (Addison–Wesley, New York, 1990).

[112] D. Dab, A. Lawniczak, J.-P. Boon and R. Kapral, Phys. Rev. Lett. 64(1990)2462.

[113] D. Dab and J.P. Boon, in: *Cellular Automata and Modeling of Complex Physical Systems,* ed. P. Manneville (Springer, Berlin, 1989), p. 257.

[114] A. Lawniczak, D. Dab, R. Kapral and J.P. Boon, Physica D, to be published.

[115] S. Wolfram, J. Stat. Phys. 45(1986)471.

[116] P. Calvin, P. Lallemand, Y. Pomeau and G. Searby, J. Fluid Mech. 188(1989)437;
V. Zehnle and G. Searby, J. de Phys. 50(1989)1083.

[117] D. Walgraef, G. Dewel and P. Borckmans, Z. Phys. B48(1982)167;
D. Walgraef, G. Dewel and P. Borckmans, J. Chem. Phys. 78(1983)3043.

[118] G.A. Bird, in: *Molecular Simulations in Complex Flows,* ed. M. Mareschal (Plenum, New York, 1990).

[119] C. Vidal and H. Lemarchand, *La Réaction Créatrice* (Hermann, Paris, 1988).

[120] T.M. Liggett, *Interacting Particle Systems* (Springer, New Tork, 1985).

[121] R. Kopelman, Science 241(1988)1620;
R. Kopelman, in: *The Fractal Approach to Heterogeneous Chemistry,* ed. D. Avnir (Wiley, New York, 1989);
C.R. Doering and D. Ben-Avraham, Phys. Rev. A38(1988)3035;
K. Lindenberg, B.J. West and R. Kopelman, Phys. Rev. Lett. 32(1988)626.